NTNU – Trondheim
Norwegian University of
Science and Technology

Underwater Radio Communication

Per Øyvind Eid Fjuk

Master of Science in Electronics
Submission date: June 2013
Supervisor: Egil Eide, IET
Co-supervisor: Torbjørn Ekman, IET
Magne Pettersen, Kongsberg Maritime

Norwegian University of Science and Technology
Department of Electronics and Telecommunications

Problem Description

The student should investigate the possibilities and limitations regarding short-range radio communication in seawater. A customized underwater node should be designed and fabricated on the basis of an implementation into a cNODE Research Midi system from Kongsberg Maritime. The node should be equipped with a radio transmitter, which can transmit a known data sequence at different data rates. The transmitter should be connected to the antennas previously made in the specialization project. A similar antenna towed from a boat passing over the node should measure signals from the submerged node. The data should be analyzed to estimate signal strength, achievable range, data rate etc. The results should be compared to theoretical values.

Preface

This thesis is submitted in partial fulfillment for the degree master of science in technology (M.Sc.) from the Norwegian University of Science and Technology in Trondheim. The work outlined in this thesis has been conducted the spring semester from 16th of January to 16th of June 2013. This thesis is based on results and products from a preceding project, 'Underwater Radio Communication using Wideband Biconical Antennas' from fall 2013 by the author. Both projects have been accomplished in cooperation with Kongsberg Maritime AS.

Acknowledgements

First and foremost, a huge thanks to Egil Eide (NTNU and 3d-Radar AS) and Torbjørn Ekman (NTNU) for being my supervisors during this thesis work. I have got all the help needed to carry through this project. Not only for theoretical work but also assisting me when conducting my experiments out in the field. Secondly, I want to thank Magne Pettersen (Kongsberg Maritime AS) and Thor S. Husøy (Kongsberg Maritime AS) for providing all the equipment necessary for this project and practical guidance. A special thanks to the guys at Trondheim Biological Station and the crew on R/V Gunnerus for giving me the opportunity to perform my measurements, both at sea and onshore on their expense. A great appreciation for all the help from Tore Landsem (IET Mechanical Workshop) for helping me out with all of my mechanical issues with my gear throughout the year, and also assisting me on the expedition at sea.

At last I want to thank my "partners in crime", André Firing, Henrik Mejlænder-Larsen and Jon Petter Skagmo, for all good times during these five years in Trondheim.

Trondheim, 16th June, 2013

Abstract

In subsea applications, there is a growing demand for high-speed wireless communication links for transmitting data between different equipment. Radio communication is constrained by the high attenuation in seawater. Only a very short range is achievable, even at low frequencies. In this thesis an independent, battery-driven radio frequency transmitter is developed and tested to investigate the properties of, and prove the concept of underwater radio communication. The transmitter is made on the basis of a cNODE Research Midi system from Kongsberg Maritime. A software-defined radio receiver is used to measure and store the received signal for post-processing. BPSK modulated data is transmitted through seawater with a 5 MHz carrier with several data rates from 237 bps to 46.598 kbps. Two tests with approximately 50 m and 11 m depths in Trondheimsfjorden have been conducted. Maximum range was measured to be close to 5 m at 9 m depth with 1 W (+30 dBm) output power. Although, this is believed to be in an area where there might be a lot of freshwater mixed in the seawater, which would in theory improve the range compared to for pure seawater. Data from the software-defined radio has been successfully demodulated with a custom made MATLAB program for all data rates, hence proven the underwater radio communication concept.

Sammendrag

I subseaindustrien er det et økende behov for høy-datarate, trådløs kommunikasjon for å sende data mellom enheter. I sjøvann er radiokommunikasjon begrenset av høy attenuasjon av signalene. I denne oppgaven er en uavhengig og batteridrevet radiosender laget og testet for å undersøke egenskapene, samt bevise konseptet radiokommunikasjon under vann. Senderen er laget med basis i et cNODE Research Midi system fra Kongsberg Maritime. En SDR-mottaker (software-defined radio) har målt og lagret det mottatte signalet for etterprosessering. BPSK-modulert data er sendt gjennom sjøvann på en 5 MHz bærebølge med ulike datarater fra 237 bps til 46.598 kbps. To tester er gjort i Trondheimsfjorden på henholdsvis 50 m og 9 m. Maksimal rekkevidde ble målt til nærmere 5 m på 9 m dybde og med 1 W utgangseffekt. Dette da på et område som kan inneholde en del ferskvann, noe som kan gi en lengre rekkevidde enn kun ved rent saltvann. Den lagrede dataen fra SDRen har blitt demodulert ved hjelp av et MATLAB-program for alle datarater, og dermed bevist konseptet undervanns radiokommunikasjon.

Contents

List of Figures

List of Tables

Abbreviations

AWGN	Additive White Gaussian Noise
BER	Bit Error Rate
BPSK	Binary Phase-Shift Keying
cPAP	Cymbal Acoustic Protocol
CDF	Cumulative Distribution Function
CTD	Conductivity, Temperature and Depth
DAC	Digital-to-Analog Converter
DDS	Digital Direct Synthesis
DP	Dynamic Positioning
EM	Electromagnetic
FPGA	Field-Programmable Gate Array
FSK	Frequency-Shift Keyeing
LPF	Low-Pass Filter
LUT	Look-Up Table
PA	Power Amplifier
QPSK	Quadrature Phase-Shift Keying
RBW	Resolution Bandwidth
RF	Radio Frequency
ROV	Remotely Operated Underwater Vehicle
SDR	Software Defined Radio
SNR	Signal-to-Noise Ratio
SPI	Serial Peripheral Interface
TBS	Trondheim Biological Station
VLF	Very Low Frequency

1 Introduction

The work outlined in this master thesis is a successor of a project thesis in the same field, underwater radio communication, from the course 'TFE4540 Specialization Project' given at NTNU. This thesis will outline EM communication through seawater, based on both theoretical work and experimental measurements in seawater. In this introduction a short background description is given first, followed by a section regarding previous work. At last the scope of the thesis is presented.

1.1 Background

An increasing amount of equipment and machines are designed and fabricated for use in subsea related applications for the petroleum industry. Extensive use of sensors, switches, and other digitally controlled units demand a high degree of surveillance and controlling abilities. These applications require a high rate digital communication to achieve required quality and performance. For subsea equipment there is a constant issue with encapsulating the parts to withstand the enormous pressure and prevent any seawater leakages. Thus, for some applications it is more practical to utilize wireless communication between different electronic equipment, as opposed to use a traditional cable communication system.

In this specific assignment, it is desirable to investigate the aspects of a high data rate wireless communication link for use between a remotely operated underwater vehicle (ROV) and a nearby subsea installation. The ROV is thought to drive around the installation collecting data, also referred to as data harvesting, from communication nodes placed around the installation. Key figures in this specific assignment are actual achievable data rate and range. The electromagnetic (EM) properties of water are mainly described from general EM theory, but it is only a limited amount of reports from actual experiments available. Most of them only measured signal strength versus range. Thus, provide a proof of concept for wireless radio/EM communication through seawater is the essence for this thesis, in addition to measure data rate and range.

1.2 Previous Work

Existing studies on EM properties of water has been investigated previously in a project thesis from the course 'TFE4540 Specialization Project' offered at NTNU. This project resulted in a report and two biconical wideband antennas, optimized for use in seawater [Fjuk 2012]. Results from experiments conducted when testing the antennas in seawater gave strong indications of successful EM communication even for significantly longer range than theoretically possible. Since the measurements was done by a network analyzer connected to the two antennas submerged in water, several possible measurement uncertainties were present. The largest concern was that the two antennas were unbalanced, which gave a possibility of current flowing on the outside of the coaxial cables connecting the antennas to the network analyzer. This current flow on the outer conductor could compromise the measurements, and thus yield wrong results. In order to overcome this issue and also remove any other possible sources of error, the two antennas should not be connected mechanically to each other in any way during measurements.

1.3 Thesis Scope

The main objectives for this assignment should be to investigate the aspects of EM-transmission through seawater. An independent submersible node should be created on the basis of commercially accessible hardware. The node should be self powered and connected to the previously made biconical antennas for underwater communication [Fjuk 2012]. Known sequences of data are to be transmitted with several data rates and modulation schemes in order to measure achievable data rate and signal-to-noise ratio (SNR) versus range. A receiver station is to be set up on a boat using the other, similar antenna, connected to a Software Defined Radio (SDR). This SDR should record the received signals directly to a hard drive for post-processing of the data. This will conserve the information in the received signal with respect to changes in phase, amplitude, and other distortions of the sent signal. The recorded signal should be analyzed and the modulated data should be decoded to both prove the concept, and gather information of seawater as a communication channel. The results are to be compared with theoretical values and results from other researchers.

2 Theory

In this chapter an overview of previous research are given first, followed by an introduction to relevant electromagnetic theory and calculations for this specific project. Afterwards different aspects concerning digital communication are presented. Most of the sections regarding literature research and EM properties of water are republished from Fjuk [2012], however with modifications.

2.1 Literature Research

2.1.1 Early Studies

The earliest scientific research in the field of underwater radio communication started with the development of submarines. In the early 1900's, communication between land and submarines were used, utilizing very low frequency (VLF) radio waves transmitted over the air and that could penetrate the seawater a few ten's of meters below the surface to a submerged submarine. VLF-frequencies are typically in the order of kHz, and hence the date rate is generally low.

Until recently, medium range (in the order of 100 m) communication with high frequencies has been considered to be impossible in general. An extensive and commonly cited article by Moore [1967] describes the different aspects with radio communication in the sea. It concludes with VLF to be the optimal possible frequency of launching a radio wave in order to communicate from land to submarines. The short skin depth (explained in the following Section 2.2.3) is given as the main reason for the VLF-frequency constraint. Several tests of radio communication under water in higher frequencies at MHz and GHz have been made, but most of them are done close to the surface. This raises a question about if the radio wave are propagating from the transmitter in the water - up in the air - and then down in the water to the receiver again. An experiment by Siegel and King [1973] measured a range up to roughly 5 m at a frequency of 5 MHz and a depth of 15 cm. In addition, they registered a variation of 10 dB because of waves in the water, which indicate that the signal path might include propagation through the air above the water.

2.1.2 Recent Studies

There has been found to be at least two research groups, which has done thorough experiments in communication in water. Al-Shamma'a et al. [2004, 2006] and Lucas et al. [2007, 2008] achieved a distance of approximately 90 meters at 1 MHz and 5.5 MHz respectively. However, the signal level attenuated close to 100 dB after just a few meters of propagation before it flattened out and maintained an almost constant signal level afterwards. According to conventional electromagnetic theory presented in the next chapter 2.2, this should not be possible because of an exponential attenuation curve (linear in dB-scale). This-flattening attenuation phenomenon is further discussed in the following Section 2.1.3.

2.1.3 Medium Range Phenomenon

A few experiments done by several independent research teams have measured a much longer propagation range that does not agree well with conventional electromagnetic theory. The attenuation of radio signals given in Figure 2.3 and the skin depth in Figure 2.5 indicates an exponential attenuation with respect to distance. Thus, no long-range propagation should be expected. However, an old notice in Wireless World from 1966 reports measured radio signals at a distance of roughly 450 meters at 76 m depth in the pacific outside San Francisco [Northrup Corporation 1966]. The article also comments that the transmission where not changing with changes in depth, which would be expected if the propagation path was by sea-air-sea. This medium range phenomenon is not widely investigated even today, despite the discovery reported in Wireless World from 1966. In more recent time, Shaw et al. [2006] has reported a measured range of roughly 90 meters in the Liverpool marina, with 5 W (+ 37 dBm) output power and a frequency around 5 MHz. However, the depth was less than 5 meters, so the question whereas the propagation path is through air still remains unanswered. The measured results from Shaw et al. [2006, p. 574] are republished in Figure 2.1. Lucas and Yip [2007] have measured a propagation distance of 85 meters in the Liverpool Dock with approximately the same parameters. This flattening attenuation phenomenon and achieved long range contradict the conventional EM theory presented in the next Section 2.2. The reason for this sudden improvement in range is not known, although Al-Shamma'a et al. [2004] claims that this is due to a change in the waters electromagnetic behavior.

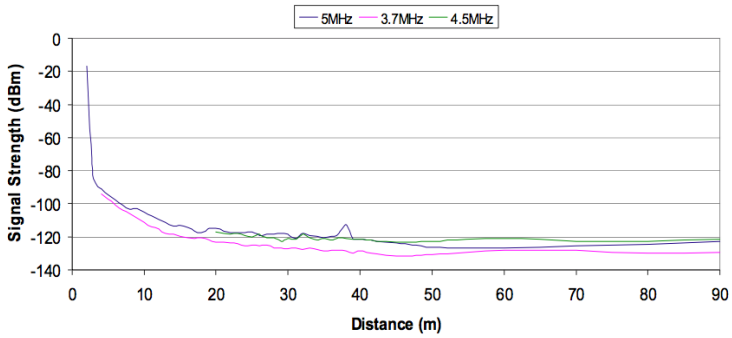

FIGURE 2.1: Measured Signals in Seawater at the Liverpool Marina.

2.1.4 Commercial Products

There exist at least one company that has specialized their products around EM communication in seawater. WFS Technologies Ltd from Scotland offers three different modems for short-range communication. The specifications vary between the products, but the longest range is about 40 m with an external loop antenna, and 100 bps. The highest data rate is stated to be up to 156 kbps for a range of 5-7 m [WFS Technologies 2012]. The system uses about 10-12 W extra when transmitting, but the effective output power from the antennas is substantially lower than that due to heat dissipation in the power amplifier. The frequencies used in these products are unknown, although their patent [Rhodes & Hyland 2009] covers all frequencies between 10 Hz to 1 MHz. A drawing from their patent application with the use of coil antennas is republished in Figure 2.2.

2.2 Propagation in water

2.2.1 Wave Equation

Propagation of electromagnetic signals in water is quite different compared to propagation in air. Parameters such as permittivity (ε) and conductivity (σ) gives strong changes in the way an EM-wave propagates through the medium. The wave equations from Maxwell's fundamental equations for a harmonically varying electromagnetic field is given by this formula [Ulaby, Michielssen & Ravaioli 2007]:

$$\nabla^2 \tilde{E} + k_0^2 \varepsilon_r \mu_r \tilde{E} = 0 \ [\mathrm{V\,m^{-1}}] \tag{2.1}$$

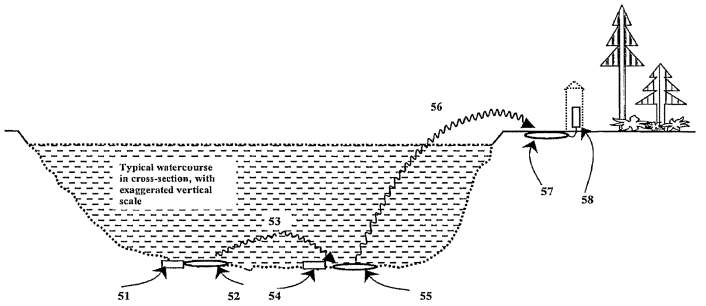

FIGURE 2.2: Underwater Communication Patent Drawing. Including EM Communication to an Onshore Base.

$\tilde{E}$ is the vector phasor for the time-harmonic electric field E, k_0 is the wavenumber and ε_r and μ_r is the relative permittivity and permeability respectively. The relative permeability μ_r is approximately the same in air and sea equal to 1, but the relative permittivity ε_r is not. Usually, the relative permittivity in air is kept constant and equal to 1, while in water this changes to be varying with several other factors like temperature, salinity/conductivity and frequency. From Ellison et al. [1998] the relative permittivity in seawater can be estimated close to:

$$\varepsilon_r = \varepsilon' + j\varepsilon'' = 72 + j39 \text{ [unitless]} \tag{2.2}$$

The permittivity of free space ε_0 is equal to 8.85×10^{-12} F m^{-1}, while the relative permittivity ε_r depends on the medium (ε_r in air is 1). Permittivity in general is defined as a real component in lossless media such as air, but in this case the seawater is a lossy media with a conductivity σ not equal to 0, resulting in the permittivity to become a complex term (in addition the the complex relative permittivity).

$$\varepsilon = \varepsilon' + j\varepsilon'' = \varepsilon_r\varepsilon_0 + j\frac{\sigma}{\omega} \text{ [F m}^{-1}\text{]} \tag{2.3}$$

Conductivity σ is in a perfect dielectric material equal to zero and in a perfect conductor close to infinite. For all practical purposes the conductivity in free air is zero, while it is a positive number in a lossy medium such as water. For example the conductivity in freshwater is close to 0.02 S, while it is as large as 4 S in pure seawater. The large variation in conductivity is mainly due to the salinity of the two different water types, where a high grade of salinity gives high conductivity [Ellison, Balana, Delbos, Lamkaouchi, Eymard, Guillou & Prigent 1998]. The seawater close to the surface might be somewhat mixed with freshwater from creeks and rivers, and thus having a conductivity somewhere between 0.02 S and 4 S.

The wavenumber k_0 is defined as:

$$k_0 = \omega\sqrt{\mu_0\varepsilon_0}\ [\mathrm{rad\,m^{-1}}] \tag{2.4}$$

ω is the angular frequency equal to 2π divided by the frequency ($\omega = \frac{2\pi}{f}\ \mathrm{rad\,s^{-1}}$). With the wavenumber inserted in the first wave Equation (2.1), the new expression becomes:

$$\nabla^2\tilde{E} + \omega^2\varepsilon\mu\tilde{E} = 0 \tag{2.5}$$

Solutions to (2.5) are given in [Ulaby et al. 2007, p. 334] for the negative z-direction;

$$\tilde{E}(z) = \hat{x}\tilde{E}_x(z) = \hat{x}E_{x0}e^{-\gamma z} = \hat{x}E_{x0}e^{-z(\alpha+j\beta)} \tag{2.6}$$

Where $\gamma = \alpha + j\beta$ is known as the attenuation coefficient, with α and β given as:

$$\alpha = \omega\left\{\frac{\mu\varepsilon'}{2}\left[\sqrt{1+\left(\frac{\varepsilon''}{\varepsilon'}\right)} - 1\right]\right\}^{\frac{1}{2}}\ [\mathrm{Np\,m^{-1}}] \tag{2.7}$$

$$\beta = \omega\left\{\frac{\mu\varepsilon'}{2}\left[\sqrt{1+\left(\frac{\varepsilon''}{\varepsilon'}\right)} + 1\right]\right\}^{\frac{1}{2}}\ [\mathrm{rad\,m^{-1}}] \tag{2.8}$$

α and β is the attenuation- and phase constant of the medium respectively. Notice both of them increases with frequency in the term ω at the start of the expression.

In order to visualize the effect of the various permittivities and conductivities for different mediums, a normalized version of formula (2.6) is presented graphically in Figure 2.3 for air, freshwater and seawater for a frequency of 5 MHz. This is the same frequency Shaw et al. [2006] and Lucas et al. [2007] used when experiencing the medium range phenomenon. As can be observed from the figure, the E-field attenuation in water decays rapidly in seawater compared to freshwater and air. This means that the radio signals in seawater should in theory have a very limited range in the order of a meter.

2.2.2 Dielectric Loss Tangent

The ratio of the real and complex part of the permittivity is commonly referred to as the dielectric loss tangent and is defined as:

$$\tan\delta = \frac{\varepsilon''}{\varepsilon'} = \frac{\sigma}{\varepsilon_0\varepsilon_r\omega}\ [\mathrm{unitless}] \tag{2.9}$$

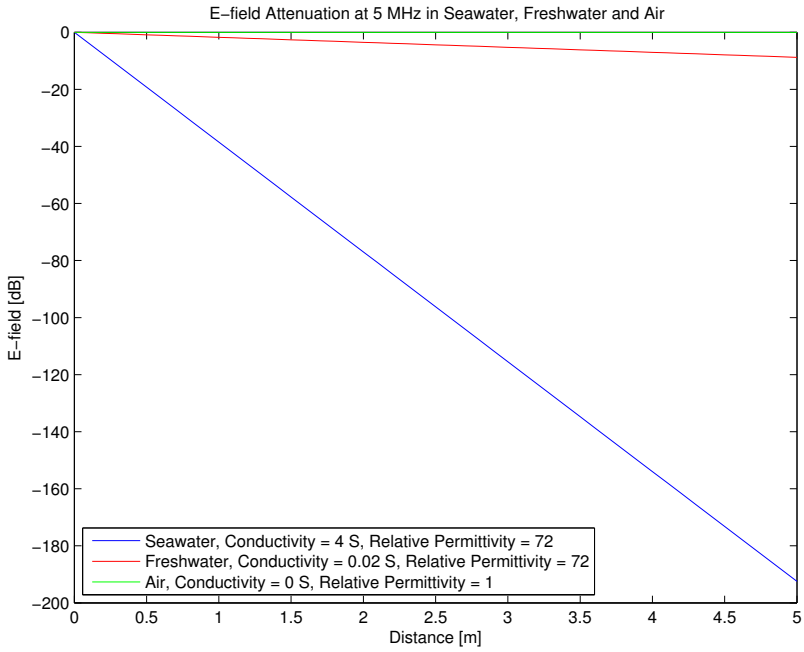

FIGURE 2.3: E-field Attenuation in Seawater.

In general, the loss tangent can infer if the medium is either a 'good conductor' or a 'low-loss dielectric', determined if the $\tan\delta$ is either a high value ($\gg 10^2 = 100$) or a low value ($\ll 10^{-2} = 0.01$) respectively [Ulaby et al. 2007, p. 335]. These two characterizations give the opportunity to simplify the expressions for α and β if the dielectric tangent is either a small or large value as shown in below:

$$\begin{aligned} \tan\delta \gg 10^2 = 100 \quad &\longrightarrow \quad \text{Good Conductor} \\ \tan\delta \ll 10^{-2} = 0.01 \longrightarrow \quad &\text{Low-loss Dielectric} \end{aligned} \tag{2.10}$$

If the value of $\tan\delta$ is in the middle between these two characterizations, the medium is commonly described as a 'quasi-conductor' [Ulaby et al. 2007, p. 335]. As can be seen from Figure 2.4 plotting $\tan\delta$ for different conductivities, the seawater can be considered to be a quasi-conductor for a frequency in the lower MHz-band. Since the dielectric loss tangent is dependent on the conductivity, which is maybe not equal to 4 S in the seawater close to the surface, the expressions for α and β (Equation 2.7 and 2.8) should not be simplified.

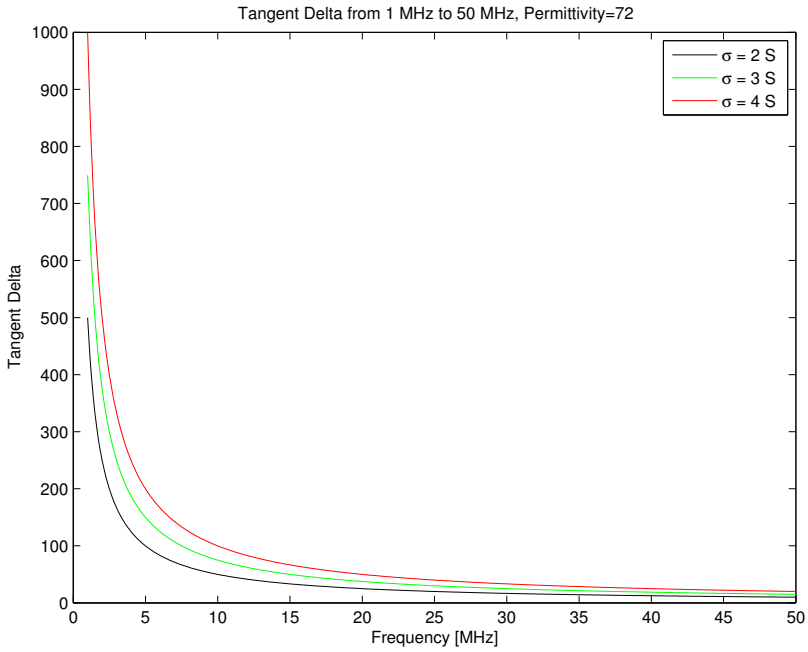

FIGURE 2.4: Dielectric Loss Tangent from 1 MHz to 50 MHz.

2.2.3 Skin Depth

The skin depth δ_s characterizes how deep an EM-signal can penetrate into a conductive medium [Ulaby et al. 2007, p. 334]. More precisely, it is the distance it takes before a normalized EM signal attenuates down to a magnitude equal to $e^{-1} \approx 0.37$. Put in context with Equation (2.6) for the EM signal:

$$|\tilde{E}_x(z)| = |E_{x0}e^{-z(\alpha+j\beta)}| = |E_{x0}e^{-\alpha z}e^{-j\beta z}| = |E_{x0}|e^{-\alpha z} \tag{2.11}$$

Normalizing the EM field and setting it equal to e^{-1}:

$$\frac{|\tilde{E}_x(z)|}{|E_{x0}|} = \frac{\cancel{|E_{x0}|}e^{-\alpha z}}{\cancel{|E_{x0}|}} = e^{-\alpha z} = e^{-1} \tag{2.12}$$

Thus the skin depth δ_s is the distance z equal to:

$$\delta_s = \frac{1}{\alpha} \text{ [m]} \tag{2.13}$$

Notice that the skin depth is heavily dependent on the conductivity (σ_s) of the medium. E.g. in a perfect conductor where the conductivity is defined as infinite ($\sigma = \infty$), the skin depth approximates down to zero ($\delta_s = 0$) and no EM-signal can penetrate the medium. This effect is used in coaxial cables where the signal cannot (ideally) penetrate the outer shielding and hence no loss in the signal is experienced traveling through the cable [Ulaby et al. 2007, p. 334]. On the other way around for a perfect dielectric where the conductivity is zero ($\sigma = 0$), the skin depth goes to infinity ($\delta_s = \infty$). Thus the EM signal can in theory travel an indefinitely long distance without any attenuation. Figure 2.5 plots the skin depth defined in Equation 2.12 for seawater at from 100 kHz to 5 MHz and with different conductivities. As can be seen from the figure, seawater

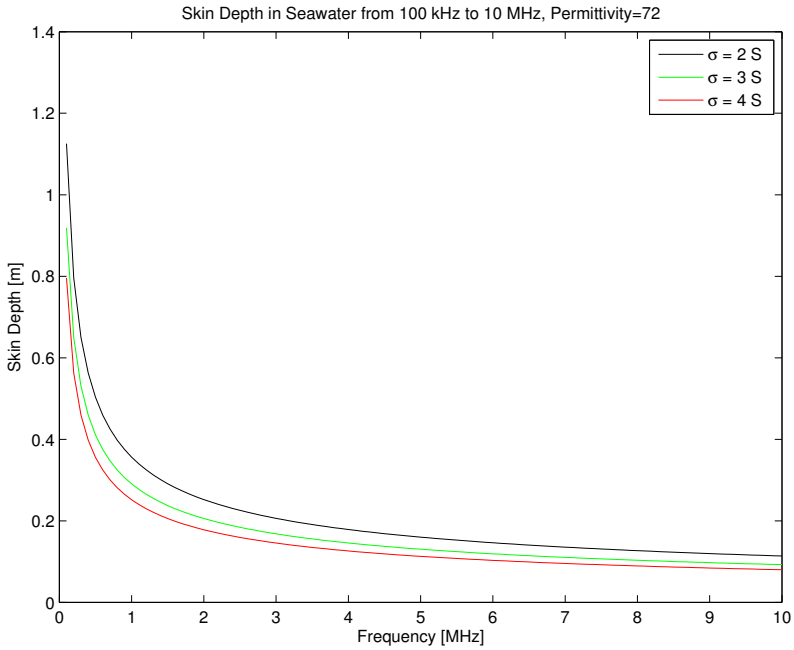

FIGURE 2.5: Skin Depth in Seawater.

has a very short skin depth, in the MHz-regime. This indicates that seawater is not suitable for radio wave propagation for frequencies in the MHz-regime due to high attenuation. Notice the large improvement at the lowest frequencies. This seems to give a decent range, however the tradeoff is a lower data rate achievable. This relation is discussed in Section 2.4.7.

2.3 Link Budget

2.3.1 Link Budget Between Two Points

A link budget characterizes the loss in signal strength through a radio transmission channel in a specified medium. The link budget, or commonly known as "The Friis Equation" [Balanis 2005, p. 94], expresses the ratio of received-to-transmitted-power ratio in terms of antenna gain, wavelength, permittivity, impedance mismatch, polarization mismatch etc. Basically all parameters that have any effect on the sent signal on its path from the output of the transmitter through a medium, and into the receiver are taken into the calculation. The linear- and dB-scale version of the link budget is given below in formula (2.14) and (2.15) respectively:

$$\frac{P_{RX}}{P_{TX}} = \left(1 - |\Gamma_{RX}|^2\right)\left(1 - |\Gamma_{TX}|^2\right) G_{RX} G_{TX} \left(\frac{\lambda_r}{4\pi R}\right)^2 \frac{e^{-\gamma R}}{L_a} \tag{2.14}$$

$$\begin{aligned} P_{RX}\ [\text{dBW}] - P_{TX}\ [\text{dBW}] &= \left(1 - |\Gamma_{RX}|^2\right)\ [\text{dBi}] + \left(1 - |\Gamma_{TX}|^2\right)\ [\text{dBi}] \\ &+ G_{RX}\ [\text{dB}] + G_{TX}\ [\text{dB}] - 2\left(\frac{4\pi R}{\lambda_r}\right)\ [\text{dB}] - L_a\ [\text{dB}] + e^{-\gamma R}\ [\text{dB}] \end{aligned} \tag{2.15}$$

P_{RX} and P_{TX} are the received and transmitted power respectively. $(1 - |\Gamma_{RX}|^2)$ and $(1-|\Gamma_{TX}|^2)$ accounts for impedance mismatch in the antennas, while G_{RX} and G_{TX} represents the antenna gain for the receiving and transmitting antenna respectively. L_a summaries all other losses thinkable, such as cable loss, polarization mismatch, etc. The $\left(\frac{\lambda_r}{2\pi R}\right)^2$-factor is commonly known as the free space path loss (FSPL) and accounts for signal degradation of a EM wave diffusing into free space, hence the term is proportional to R^{-2} where R is the range between the antennas. The λ_r is the relative wavelength. In a lossy medium, the wavelength decreases due to the change in permittivity. The new wavelength is called the relative wavelength λ_r, which is equal to the wavelength in vacuum λ_0 divided by the square root of the relative permittivity ε_r (only the real part is considered):

$$\lambda_r = \frac{\lambda_0}{\sqrt{\varepsilon_r}}\ [\text{m}] \tag{2.16}$$

γ is the attenuation coefficient defined in Section 2.2, as:

$$\gamma = \alpha + j\beta \tag{2.17}$$

In a system where the antennas are identical, meaning $G_{RX} = G_{TX} = G$ and $\Gamma_{RX}^2 = \Gamma_{TX}^2 = \Gamma$, Equation (2.14) reduces to:

$$\frac{P_{RX}}{P_{TX}} = \left(1 - |\Gamma|^2\right)^2 G^2 \left(\frac{\lambda_r}{4\pi R}\right)^2 \frac{e^{-\gamma R}}{L_a} \tag{2.18}$$

In dB-scale:

$$\begin{aligned} P_{RX}\ [\text{dBW}] - P_{TX}\ [\text{dBW}] = 2\left(1 - |\Gamma|^2\right)\ [\text{dB}] + 2G\ [\text{dBi}] \\ -2\left(\frac{4\pi R}{\lambda_r}\right)\ [\text{dB}] - L_a\ [\text{dB}] + e^{-\gamma R}\ [\text{dB}] \end{aligned} \tag{2.19}$$

2.3.2 Thermal Noise Power

The random motion of charge carriers through a lossy medium creates thermal noise [Pozar 2001, p. 74]. The noise power P_n is defined as:

$$P_n = kTB_W\ [\text{W}] \tag{2.20}$$

k is Bolzmanns constant ($k = 1.380 \times 10^{-23}\ \text{J K}^{-1}$), T is the temperature of the lossy medium in kelvin (K), which is approximately 273 Kelvin at 0° °C. B_W is the bandwidth of the signal/frequency band of interest measured in hertz (Hz). For measurement apparatus, this bandwidth is often referred to as resolution bandwidth (RBW), indicating the bandwidth that is being measured.

Other types of EM noise can also occur, e.g. shot noise, but these sources of noise are not going to be investigated any further in this thesis.

2.3.3 Signal-to-Noise Ratio (SNR)

SNR can be defined in several ways. Basically, it is exactly what it sounds like, a ratio between the measured signal power P_{RX}, and the noise power P_n present. With respect to the link budget in formula (2.14) and (2.18) by solving these for P_{RX}, the SNR would then be:

$$SNR = \frac{P_{RX}}{P_n} = \frac{P_{TX}\left(1 - |\Gamma|^2\right)^2 G^2}{kTB_W} \left(\frac{\lambda_r}{4\pi R}\right)^2 e^{-\gamma R} \tag{2.21}$$

In digital communication a data stream consists of a sequence of bits sent through a communication channel with a certain rate, commonly known as data rate D_R (Symbols/s). Since the digital signal sends out bits sequentially, it is more convenient to define the SNR with respect to the total energy used in a

time interval and the number of bits sent in the same interval. Hence, the SNR in digital communication is defined as:

$$SNR = \frac{E_b D_R}{N_0 B_W} \text{ [unitless]} \tag{2.22}$$

Here E_b is the energy used per bit (J), typically equal to the amplitude of the carrier wave squared ($E_b = A^2$). N_0 is the thermal noise power per hertz ($N_0 = kT$ [$\mathrm{W\,Hz^{-1}}$]). This ratio is also commonly referred to as the bit energy-to-noise density [Rappaport 2002, p. 664]. Given the digital signal is binary phase-shift keying (BPSK) modulated (explained more thoroughly in the next Section 2.4.2), the bandwidth of the signal can in theory be found to be twice the data rate [Rappaport 2002, p. 296]. Next, assume the system to be very simple and non-ideal, and also let the bandwidth be approximated to be the same as the data rate ($B_W = D_R$), then the SNR becomes:

$$SNR = \frac{E_b D_R}{N_0 B_W} = \frac{E_b B_W}{N_0 B_W} = \frac{E_b}{N_0} \text{ [unitless]} \tag{2.23}$$

2.4 Digital Communication

Any transferable signal containing information/bits has to be distinguishable for the receiving part in order to decode any information in the signal properly. In general, one or several bits grouped together are mapped on to an symbol. The number of symbols has to be equal to the number of possible uniquely grouped sequence of bits. An S denotes the unit of a symbol, and n the number of bits contained in each symbol. The number of unique sequences/symbols of the n-bits becomes:

$$\text{Number of Symbols } = 2^n \text{ [S]} \tag{2.24}$$

This mapping of bits onto a signal is called modulation, and can be done in numerous ways. E.g. assigning different voltages, power levels, or in time slots. It is important for both the transmitter- and receiver-side to agree of what kind of modulation that is done, and which bits the symbols represents in order to retrieve/demodulate the information contained in the signal.

The probability of demodulating a received signal into a wrong symbol and in the end a wrong bit, is commonly denoted as P_e (probability of bit error). The goal of any transmission is to send over all the information from the transmitter to the receiver flawlessly. In other words, it is desirable to keep the P_e as low as possible, ideally zero. The trade-off here is generally energy, and/or time used for sending the signals to achieve a tolerable probability of error. The P_e is a

theoretical figure which can be derived mathematically for the given modulation type from general probability theory.

2.4.1 Channel Noise

When all signals is transmitted through a lossy medium such as air, metal, or in this case water, the shape of the signal might be deformed or distorted due to phenomenas such as attenuation, thermal noise, etc. Because of this deformation effect, the signal could transform in a way that make the sent symbol looks like a different symbol when it is received. E.g. the modulated version of a binary "0" could look like a "1", resulting in a error in the demodulation. Since there exists very little information about the characteristics of the channel noise in seawater, an assumption is made that the noise is white and with a Gaussian probability distribution (independent and identically distributed random variables) with a mean $\alpha = 0$ and a standard deviation $\sigma^2 = {}^{N_0}/_2$. This noise $n(t)$ is assumed to add with the originally sent signal $x(t)$, and sums up to the received signal $y(t)$. I.e.:

$$y(t) = x(t) + n(t) \tag{2.25}$$

This type of channel noise is often referred to as additive white Gaussian noise (AWGN) and is a common noise model in digital communication theory [Proakis & Salehi 2008, p. 160, 358]. A graphical representation of the AWGN channel is given in Figure 2.6.

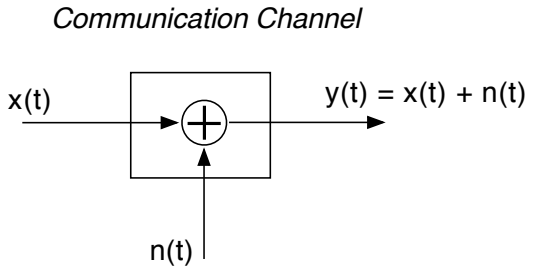

FIGURE 2.6: Additive White Gaussian Noise Channel.

2.4.2 Binary Phase-Shift Keying (BPSK)

One of the most basic modulation technique/scheme for wireless communication is BPSK. It is called binary since only two symbols are used, transmitting one

bit at the time. In general, phase modulation is based on sampling the carrier wave at specific times, and by looking at the phase of the sinusoidal carrier to determine the symbol transmitted. Figure 2.7 shows a plot of a cosine wave with amplitude A, and the corresponding polar mapping with the constellation with two BPSK symbols. In this specific case, the '0' and '1' bits are at A and $-A$ respectively. The two points differ with 180 degrees in phase, hence phase modulation. A sample of a BPSK modulated waveform and the corresponding bits are shown in Figure 2.8. When a signal is sampled, it can be mapped in the diagram below and the closest constellation point/phase, will determine which symbol to be assigned to it. This detection technique is commonly called a *nearest neighbor/*, or a *minimum-distance* detector [Proakis & Salehi 2008, p. 171], referring to the Euclidean distance between constellation points in Figure 2.7. This modulation technique requires coherent detection [Couch II 1995, p. 378], meaning that the sampling must be synchronized at the start when the signal first reaches the receiver. Several more constellation points can be assigned to the diagram,

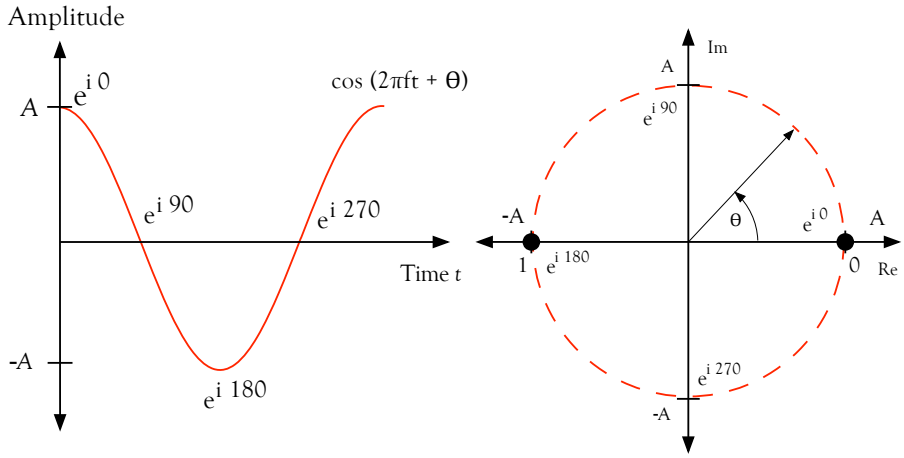

FIGURE 2.7: BPSK Mapping and Constellation Diagram.

giving an higher order of modulation. If two more points are used, the circle gets divided into four equally spaced line segments and two bits get packed in each symbol transmitted. This scheme is called 4-PSK or quadrature phase-shift keying (QPSK), where there are 4 different symbols (ref. Equation 2.24, $n = 2$). The tradeoff is a lower tolerance for any influence by the communication channel. Each sent symbol is more vulnerable for any noise, etc. since the geometrical distance to another constellation point is smaller. Hence the probability of detecting the wrong symbol gets higher [Proakis & Salehi 2008, p. 193]. Surprisingly, the

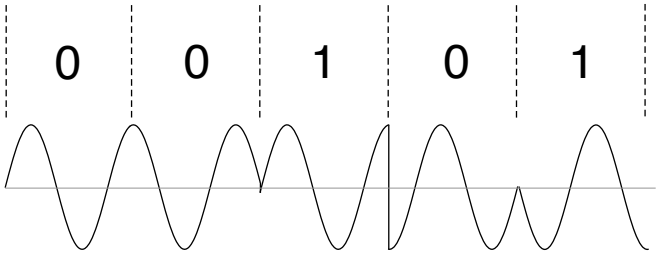

FIGURE 2.8: BPSK Waveform.

probability of bit error is equal for both QPSK and BPSK due to the fact that two bits gets transmitted in one symbol [Rappaport 2002, p. 300] and the symbols is orthogonal onto the closest symbol constellation points [Proakis & Salehi 2008, p. 193]. The probabilities of errors for the two schemes are given in Table 2.1. Increasing the amplitude of the signal, and making the circle larger can be done as a countermeasure to control the probability of symbol error. In other words, increasing the SNR ratio. In theory, it is possible to use as many constellation points as desired to transmit many bits (increasing the data rate) per symbol, as long as the SNR at the receiver is high enough.

2.4.3 Frequency Shift Keying (FSK)

FSK uses a change in frequency instead of phase as for PSK modulation. The main principle of this modulation is to switch between different carrier frequencies, also called tones, to send out the different symbols. The two tones have to be sufficiently separated in frequency in order to be both distinguishable and also not create any interference with each other. For the simplest case with two tones, each of the tones corresponds to a '0' or '1'. This technique is called binary FSK (BFSK). To detect the different symbols, the radio frequency (RF) input can be correlated with locally generated tones with the same frequencies, and the tone that correlates best indicates the symbol transmitted at that specific time interval. A sample of the waveform with is shown in Figure 2.9. In the opposite of PSK, FSK can use non-coherent detection [Rappaport 2002, p. 312], and thus it does not necessarily require synchronization of the sampling.

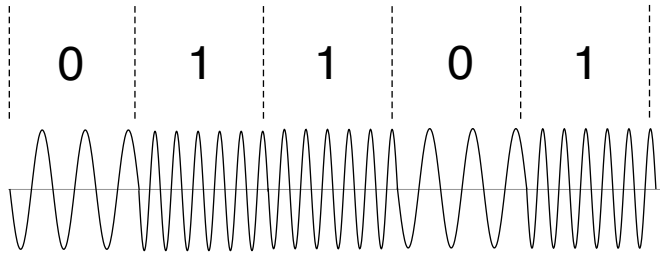

FIGURE 2.9: BFSK Waveform.

2.4.4 Bit Error Rate (BER)

The BER is a figure of measure in most communication systems. This parameter is based on the actual statistical performance of a communication system, indicating how many bits that are wrong in a demodulated bit stream received in a time interval. While P_e is a theoretical figure, BER is the actual performance measured. This parameter can be estimated in forehand by calculating the P_e from a given modulation, and noise model. Figure 2.11 shows the P_e versus SNR (ref. Section 2.3.3, SNR= $^{E_b}/_{N_0}$) for different modulation schemes. The P_e for each modulation scheme can be derived mathematically from general probability theory, assuming the channel noise to have a Gaussian probability distribution (ref. Section 2.4.1). The different symbols are also assumed to have be equiprobable, meaning the probability of receiving the different symbols is equal. A list of P_e for several modulation schemes can be found in Coach II [1995, p. 378]. The four most relevant P_e for this project are listed in the Table 2.1 The Q-function

TABLE 2.1: Probability of Bit Error for Different Modulation Schemes.

Modulation Type	**Probability of Bit Error**	**Detection Type**
BPSK	$P_e = Q\left[\sqrt{2\left(\frac{E_b}{N_0}\right)}\right]$	Coherent
QPSK	$P_e = Q\left[\sqrt{2\left(\frac{E_b}{N_0}\right)}\right]$	Coherent
FSK	$P_e = Q\left[\sqrt{\left(\frac{E_b}{N_0}\right)}\right]$	Coherent
FSK	$P_e = \frac{1}{2}e^{-(1/2)(E_b/N_0)}$	Noncoherent

represents the probability/area of the tail from the cumulative distribution func-

tion (CDF) of a Gaussian distribution [Couch II 1995]:

$$Q(z) \equiv \frac{1}{\sqrt{2\pi}} \int_z^\infty e^{-\lambda^2/2}\, d\lambda \tag{2.26}$$

This probability decreases as the argument of the Q-function increases, as indicated in Figure 2.10. Thus, the highest argument gives the lowest probability of error.

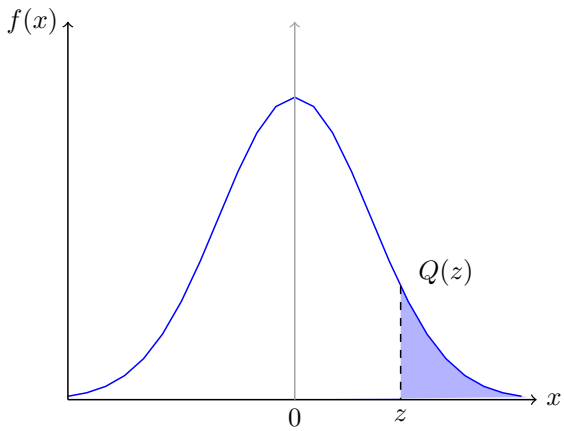

FIGURE 2.10: Q-function.

A graphical representation of the bit error probabilities is provided in Figure 2.11.As can be inferred from the diagram, a higher order modulation demands a stronger SNR in order to have an equal P_e as the lower order modulations. The BER can be improved by e.g. lower the P_e (by changing modulation scheme) or applying channel coding of the symbols.

2.4.5 Repetition Coding

To improve the bit error probability, the same bit/symbol can be sent several times. The idea in this type of coding is based on the noise is averaged out since the variance gets divided by n [Madhow 2008, p. 83], and the detector can evaluate the average received value to determine the symbol sent. In practice, the detection is based on the same technique as described in Section 2.4.2. The only difference is that all of the Euclidean distances to each symbol are summed up and then the lower of the two sums reveals the symbol bit in average. This

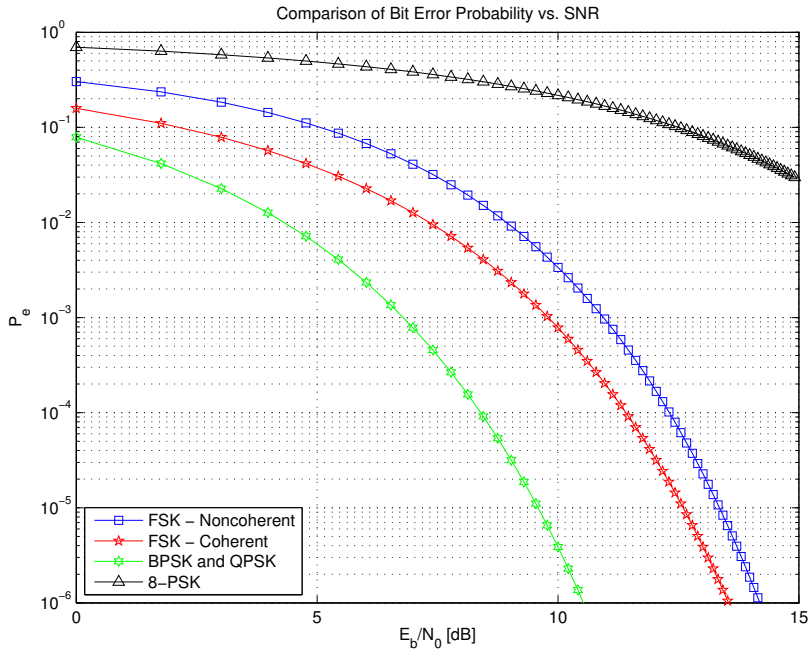

FIGURE 2.11: Bit Error Probability vs. SNR for Different Modulation Schemes.

repetition technique is a type of *block coding*, and in this specific case each block consists of the same symbols, and hence called *repetition coding*. The probability of symbol error can be found to be [Proakis & Salehi 2008, p. 429]:

$$P_{symbol} = Q\left[\sqrt{2\left(\frac{E_{symbol}}{N_0/n}\right)}\right] = Q\left[\sqrt{2\left(\frac{nE_{symbol}}{N_0}\right)}\right] \tag{2.27}$$

This n-factor increases the argument in the Q-function, and thus the probability of error will go down. In the same time, the energy used to send each symbol E_{symbol} is the sum of the energy used to send one symbol. In the BPSK case, the $E_{symbol} = \frac{E_b}{n}$. The resulting probability of bit error becomes:

$$P_e = Q\left[\sqrt{2\left(\frac{n^{E_b/n}}{N_0}\right)}\right] = Q\left[\sqrt{2\left(\frac{E_b}{N_0}\right)}\right] \tag{2.28}$$

Thus, the probability of bit error in repetition coding does not change from conventional single bit transmission as presented in Table 2.1. However, it

is convenient to use repetition coding in a comparison of data rate point of view. Since the number of repetitions corresponds to the relative increase in data rate between repetition code and single bit transmission, the two techniques should perform the same way. The same relation of P_e and repetition coding applies to QPSK and FSK as well [Proakis & Salehi 2008, p.429].

2.4.6 Sampling Theory

In order to receive and store any signal, the signal values has to be sampled a sufficient amount of times for a given time period in order to conserve the information in signal. In wireless communication, the carrier frequency might be in the order of several GHz. Fortunately, only the modulation witch has a much smaller frequency has to be sampled in order to retrieve the information sent over the communication channel. A commonly known theorem from communication theory states that the sampling frequency, fs (popularly called the Nyquist frequency), has to be at least equal two times the bandwidth of the signal [Couch II 1995, p. 100] to collect the data error free:

$$f_s \geq 2B_W \text{ [Hz]} \tag{2.29}$$

For BPSK, the bandwidth of the signal is twice the data rate [Rappaport 2002, p. 296].

$$BW_{BPSK} = 2R \text{ [Hz]} \tag{2.30}$$

For FSK on the other hand, it is a bit different since it uses two frequencies/tones. The transmission bandwidth is then also dependent of the difference between the two tones, denoted by ΔF. This effective transmission bandwidth turn out to be [Rappaport 2002, p. 313]:

$$BW_{FSK} = 2\Delta f + 2R \text{ [Hz]} \tag{2.31}$$

2.4.7 Channel Capacity

Shannon's channel coding theorem states that there exists an upper limit of possible transferable data rate for a given bandwidth and SNR. This maximum data rate is known as the channel capacity (C) is defined as:

$$C = B_W \log_2 (1 + SNR) \text{ [bits s}^{-1}\text{]} \tag{2.32}$$

This maximum capacity is a theoretical limit that does not give any indication of how to achieve this data rate in real systems. However, by utilizing

complex modulation schemes and different types of coding it is possible to converge close to this maximum data rate. A graph of the channel capacity is plotted with different SNR-levels in Figure 2.12.

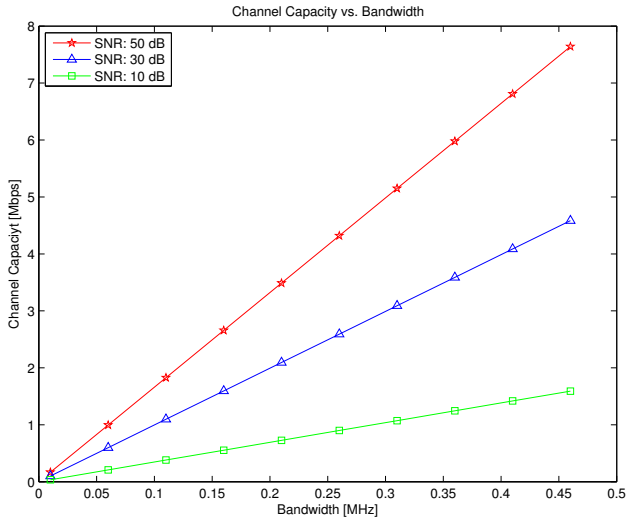

FIGURE 2.12: Channel Capacity for Different SNR.

3

System Design and Method

According to the thesis scope from the introduction chapter, the submersible transmitter node with an antenna is described below, in addition to a receiver station on the surface. An additional backup transmitter is also presented. At last, the software program for controlling the output sequences from the hardware and demodulation code for MATLAB are described in detail.

3.1 System Overview

The transmitting node hardware consists of a programmable microcontroller unit (Arduino Uno) that sends out two different binary sequences into a direct digital synthesizer (DDS) board from Mini-Kit (EME165). This synthesizer board contains a digital synthesizer from Analog Devices (AD9954) capable of generating frequencies between DC and 160 MHz with roughly +10 dBm (10 mW) output power throughout the given spectra. This signal is further amplified by a power amplifier (PA) from RF Bay (MPA-10-40) to +30 dBm equivalent to 1 W output power, which is then sent forth to the antenna and transmitted into the surrounding medium. A software-defined radio (SDR) records the measured signal strength from a similar antenna, and stores it on a hard-drive.

A carrier frequency of 5 MHz is chosen to be target since the dielectric tangent and skin depth (ref. Figure 2.4 and 2.5 respectively) are not minimal, and in the same time, the carrier is capable of transmitting with a high data rate in the order several of kbps. As mentioned previously, this is roughly the same frequency Shaw et al. [2006] and Lucas et al. [2007] used in their experiments, thus the results in this thesis should be comparable. A sketch of the concept is given in Figure 3.1.

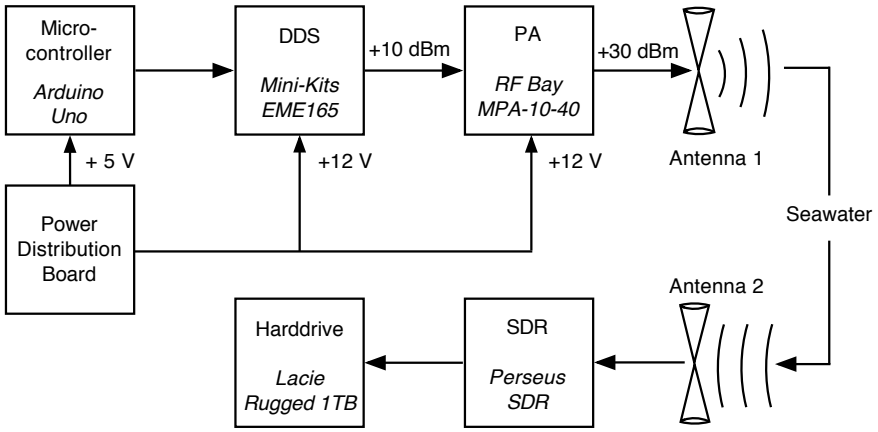

FIGURE 3.1: System Concept.

3.2 Transmitter

The custom designed hardware is cased inside a commercially available cNODE Research Midi casing from Kongsberg Maritime. A sketch of the cNODE is republished in Figure 3.2 [Pettersen & Husoey 2012]. This cNODE Research

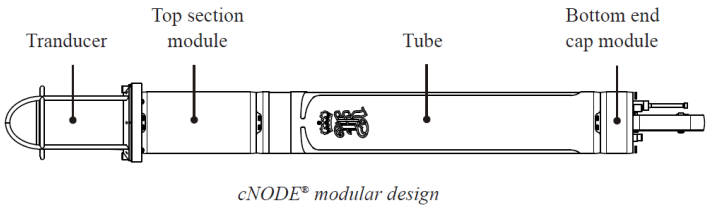

FIGURE 3.2: cNODE Research Midi Model.

Midi system contains a large battery supplying 14.4 V, an acoustic transducer, a top section module for payload and other utilities. The acoustic transducer can handle two-way communication, allowing sending commands to the cNODE and distance measurements from acoustic systems on the surface. These commands can initiate power-up/down from the internal battery and also an electrically controlled release mechanism formed as a claw. This claw is meant to hold

additional weights to keep the node safely attached to the sea floor. When the cNODE is lifted up to the surface, the claw can be opened and the weights can be released, easing the lift-up of the cNODE from the sea floor. An extra air-filled collar can also be attached to the cNODE for an automatic ascending up to the sea surface, but this is not used in this project. The whole system is shown in Figure 3.3 along with the two antennas. The acoustic system computer

FIGURE 3.3: Kongsberg Maritime cNODE Acoustic Communication System and Custom Made Antennas.

on the surface shows the range between the two acoustic transducers, and also logs them internally with a time-resolution of milliseconds. In order to determine the range between the transducers, the system uses a cPAP-protocol (Cymbal Acoustic Protocol) from Kongsberg Maritime [Kongsberg Maritime 2012]. This system can measure the range with an interval down to 0.8 seconds.

3.2.1 Power Distribution

The already built-in lithium battery in the cNODE supplies a voltage of 14.4 V. However, the different parts in the transmitter module require specific supply voltages. E.g. the microcontroller board needs 5 V, power amplifier 12 V, etc. In addition, the synthesizer board should have a 500 mA fast-blow fuse to ensure that most of the circuits and chips are protected in case of malfunctioning components or an electrical short. In order to meet these requirements from the parts, an extra power distribution board has been made (shown in Figure 3.4). The hardware on the board consists primarily of three fast-blow fuses (2x 0.5 A

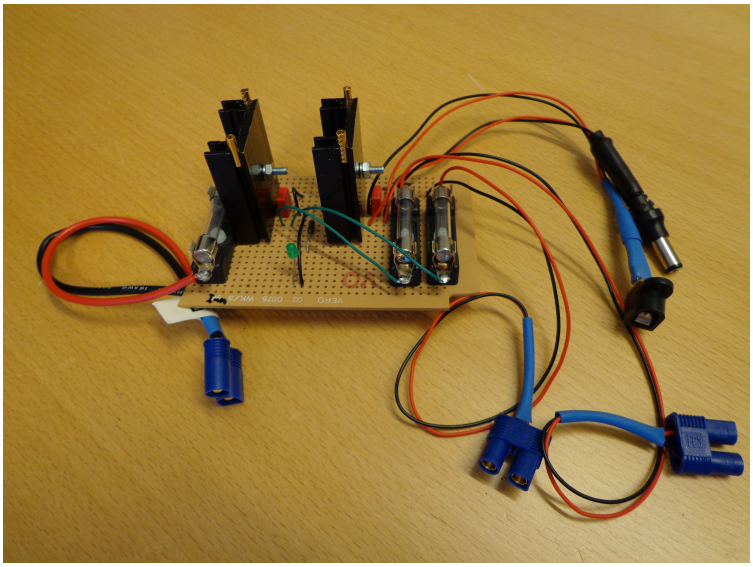

FIGURE 3.4: Power Distribution Board.

and 1x 1.5 A) and two voltage regulators that supply 5 V and 12 V (LM7805 and LM7812 respectively) from a higher voltage, in this case 14.4 V. Both of the voltage regulators are capable of giving out 1 A of supply current [Fairchild Semiconductor 2013]. All of the connectors interfacing 12 V or 14.4 V voltages are of the type EC3, while 5 V is a standard DC power jack.

3.2.2 Arduino Uno Microcontroller Board

In order to both set up and control the DDS, an Arduino Uno R3 evaluation board [Arduino 2013*a*] was chosen for this task. An Arduino board is developed as an easy platform for beginners to become experienced with programming microcontrollers. It contains an USB-port for interfacing with a computer, 5V DC female jack connector for powering, 14 digital input/output pins, 6 analog pins and a boot loader for directly programming the ATMEGA328 microcontroller chip without the need of an extra programmer.

3.2.3 Direct Digital Synthesis (DDS)

Common analogue synthesizers uses an external oscillator, and mixes the output frequency of the oscillator with multiples and fractions of it to generate a number of frequencies. The DDS architecture utilizes a look-up table (LUT) with stored sample values of a sinusoid. A DDS uses essentially a frequency-division method, to be able to have a high frequency resolution [Pozar 2001, p. 269]. In other words the output frequency can be specified with a high accuracy of many digits. Then number of available output frequencies is usually determined by the size of the LUT and the corresponding step-size in the phase accumulator (given that the DAC has an appropriate resolution). The block diagram for a simple DDS is shown below in Figure 3.5 [Pozar 2001, p. 270] and consists mostly of an controlling unit, phase accumulator (essentially an adder), LUT and a digital-to-analog converter (DAC). The frequency control-unit controls the incremental

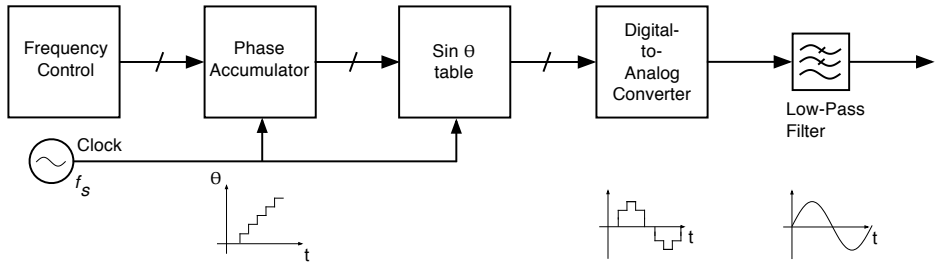

FIGURE 3.5: Direct Digital Synthesis Synthesizer Block Diagram.

value of the phase accumulator, counting the number of clock cycles with the frequency f_s. The added number from the phase accumulator is passed on to a "sin θ"-LUT which then finds the corresponding digital value of a sine wave with a similar phase. The DAC converts the digital number to an analog value/voltage,

and low-pass filter it at the output to smoothen the curve and suppress harmonics.

The EME165-board from Mini-Kits [Mini Kits 2013] contains an AD9954 (14 bit DAC) DDS chip from Analog Devices [Analog Devices 2009], in addition to several other peripheral circuits to make it easier to operate. E.g. a voltage level translator, voltage regulators, crystal clock oscillator, output filter and power amplifier. The output power from the board is roughly +10 dBm, corresponding to 10 mW.

3.2.4 Power Amplifier (PA)

The output signal from the DDS is, as mentioned previously, approximately +10 dBm. This is a relatively low output power, and makes the system vulnerable for any small mismatch losses, perturbations and other effects that might appear. The low power also makes the achievable range smaller, making it harder to detect and read the signal for a given distance compared to a higher output power (ref. the SNR Equation (2.23) and link budget Equation (2.18)). To make the system more robust and less susceptible for any small perturbations, a PA can be used to get a higher output power. A wideband MPA-10-40 linear amplifier, running on 12 V DC powering, from RF Bay was chosen [RF Bay Inc. 2013]. This PA has a typical gain of 40 dB and a maximal output power of approximately +30 dBm, corresponding to 1 W. Since the EME165 DDS board outputs +10 dBm, an additional 20 dB attenuator should be place between the two parts to avoid clipping/distortion of the signal due a too powerful input signal. A more powerful PA could be used to further increase the systems robustness and range. However, size is a constraint from the cNODE construction hence it is desirable to have a small, but powerful PA to fit into the top section module in the cNODE Research Midi system in Figure 3.2. It is also desirable to have a modest power consumption since the battery is non-rechargeable.

Another potential problem could be condensation of water inside the casing due to a powerful amplifier may give out a lot of heat. A large amount of condensated water could potentially create shorted circuits. The power efficiency in PA's tends to be relatively low, in the order of 20-50 percent. Meaning that only a fraction of the power the PA uses get sent through the output, the rest is dissipated into heat. The MPA-10-40 amplifier should use about 4.32 W when operating [RF Bay Inc. 2013], thus 3.32 W is dissipated as heat when the PA operates at its maximum. This amount of heat is quite low, and is hoped to be sufficiently low to avoid any substantial condensation problems.

The entire transmitter hardware and support construction is shown in Figure 3.6. The support structure is made of semi-rigid polyethylene. This material can easily be cut and shaped to get a compact and light structure capable

of holding the boards in a safe way. All of the electronic boards described in this section have exposed electrical connections underneath. Thus, they should not get in contact with the metal walls of the cNODE in case of any shortened connections. This complete module fits quite well into the top module section

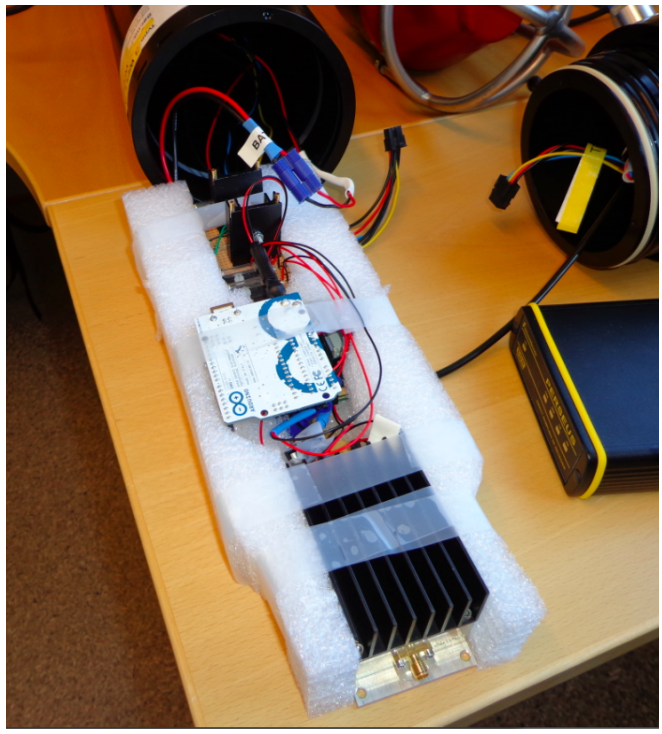

FIGURE 3.6: Transmitter Hardware and Support Structure.

shown at the picture top. In addition, two bags of water absorbing salt in case of any condensation due to heat. Several of the circuit boards have some components (voltage regulators, power transistors, etc.) that are known to get very warm and generate heat in addition to the PA.

3.3 Receiver

On the receiver side, the other antenna, acoustic transducer and weights are held by a rope from the boat and lowered down to depths of approximately the same

depth as the independent node. The signals received from the antenna is sent up to the boat by coaxial cable (RG-58) and sampled on the boat with a software-defined radio (described in the next Section 3.3.1). The recorded signal is saved as an audio file (wav-format) to be further processed on computer afterwards. This preserves the measurement data for further investigations beyond the scope of this thesis. More details of the measurement recordings are given at the end of the next section.

3.3.1 Software-Defined Radio (SDR)

In non-specific applications, hardware-based radios tend to be quite large to be able to be very agile with respect to frequencies, filters, modulation techniques, etc. These kinds of application-specific requirements can result in significant increase in complexity, area usage and labor time unless some reasonably cheap off-the-shelf product that covers the needs already exists. Along with the increasing capacity of processors and field-programmable gate arrays (FPGA), more of the signal processing has been done in the software domain to compensate for sub-optimal hardware [Chamberlain 2005]. The purpose of an SDR is to do as much as possible of the signal processing in software instead of using hardware. Typically, an SDR-radio consists of a FPGA, analog-to-digital converter (ADC), digital-to-analog convert (DAC) and an analog front-end to do mixing, band-pass filtering and power amplification.

The Perseus SDR, used in this thesis, is a wideband receiver type from Microtelecom [Microtelecom s.r.l. 2013*b*] capable of covering all frequencies between 10 kHz and 40 MHz. It has a third-order dynamic range of approximately 100 dB, and features a 14 bit, 80 MS/s analog to digital converter [Microtelecom s.r.l. 2013*b*]. This specific SDR receiver has optional sampling rates from 125 kSps (kilosamples per second) to 2000 kSps, giving an effective recordable bandwidth from 100 kHz to 1600 kHz respectively [Microtelecom s.r.l. 2013*a*]. This Perseus SDR is operated from a commercially available software from the company website [Microtelecom s.r.l. 2013*b*], allowing the user to record signals to a .wav-file and replay them as preferred to the user. The software records frequency information in order to preserve the full frequency spectrum of the entire bandwidth recorded. This record feature is mainly targeted for ham radio applications, and not necessarily for versatile radio communication. A sample of a recorded BPSK-modulated signal is presented in Figure 3.7. As can be seen from the figure, only changes in phase occur to give any large effect on the recordings. Hence, the amplitude of the modulated signal does not seem to be preserved. Instead, the magnitude and duration of the 'spikes' contains information of both amplitude and phase and makes it possible to reconstruct all of the signals in the

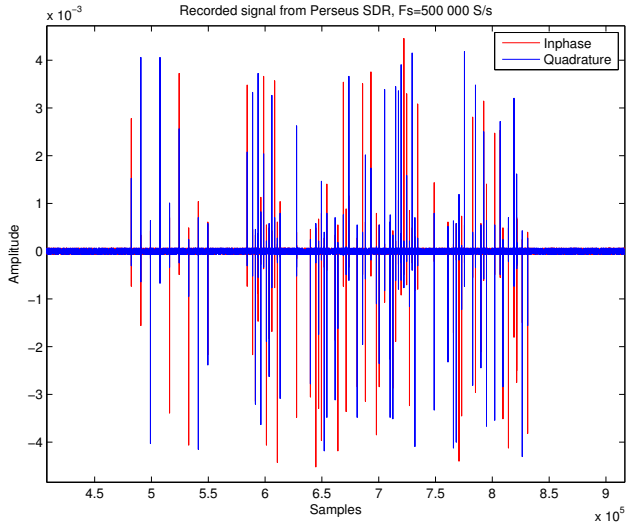

FIGURE 3.7: Perseus SDR Recordings of an BPSK Modulated Signal.

frequency spectra recorded. A method of extracting our data from this waveform is given later on in Section 3.7. The measured signal strength from the Perseus should be in ballpark the same as for other typical spectrum analyzers. The Perseus was tested against an portable spectrum analyzer (Anritsu MS2721A), and they differed only approximately 0.74 dB in their measurements. Thus, the measured signal values from the Perseus are believed to be roughly correct.

3.4 Underwater Wideband HF Antenna

Due to the different EM parameters in seawater (ref. Section 2.2) compared to air, custom-made antennas has to be used to optimize the amount of energy sent out and received trough the water. In the preceding project [Fjuk 2012] two biconical center-fed dipole antennas in brass were designed and built, in order to explore the properties of EM-waves versus frequency. Two brass cones for each antenna were encapsulated in a PVC-tube and filled with freshwater, which was supposed to give better water molecule excitation according to Yip, Goudevenos & Lucas [2008]. One of the fabricated brass antennas without the PVC-capsule is shown in Figure 3.8. The overall length of the antennas is approximately 144 cm (152 cm with PVC encapsulation), and an flare angle of roughly 10 degrees. This

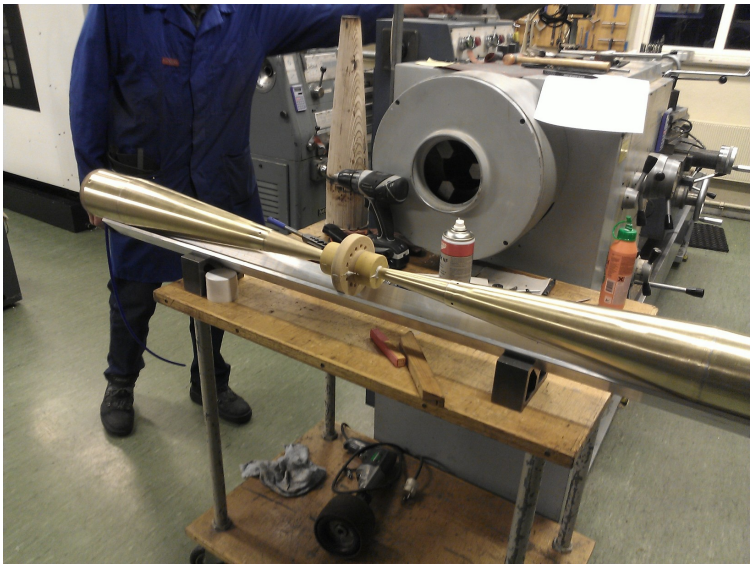

FIGURE 3.8: Custom Made Biconical Wideband HF Antenna.

yields a theoretical input impedance of about $40 - i10\,\Omega$ in seawater [Fjuk 2012]. A direct consequence of this optimization for seawater is that the antennas perform worse when tested in lab, compared to when they are in the sea. Hence, there should be expected to get somewhat different results testing the whole system in the lab versus in the sea.

The two antennas are close to identical, both in shape and size, as can be made by practical reasons. Measurements of the antennas show approximately equal behavior, hence they are assumed to be identical for all practical and theoretical purposes. Other details of the constructions and performance of the antennas can be found in [Fjuk 2012].

A RG-58 coaxial cable (with N-connectors) connects each of the two antennas to either the cNODE in the water or to the Perseus SDR receiver on the sea surface. The dipole antenna should more or less have a toroid/donut shaped radiation pattern. Meaning it radiates optimally and equally along the horizontal axis of the antenna. Hence, the measurements in the sea should be conducted with both antennas at equal depths to maximize the range.

3.5 Back-up Hardware

Due to the unknown complexity regarding programming and controlling the DDS, we determined to also have a back-up plan with a simple crystal oscillator and BPSK-modulator to ensure the transmission of a modulated signal in the frequency area of interest. This was also going to be a back-up plan in case of the primary system with the DDS would not work properly while conducting measurements out in the sea. Since we knew in forehand we had a limited time on the boat, any hardware or software modifications such as debugging the DDS should be kept to a minimum. It was also some uncertainty involved in case the DDS turned out to be hard to program and control, thus not getting the HW running in time for sea test.

The final circuit board is shown in Figure 3.9 and consists mainly of an crystal oscillator, low-pass filter (LPF), an high-speed RS-232 driver/receiver (ADM232AANZ [Analog Devices 2010]) with required peripheral components. The crystal oscillator (IQXO-350, 5 MHz [IQD Frequency Products 2012]) generates a noisy square wave signal with a frequency of roughly 5 MHz. This signal is sent through a LPF, with cut-off frequency of roughly 8 MHz, to smoothen the curve to an approximate sine wave to be the carrier wave. This carrier signal is passed on to a BPSK modulator from Mini-Circuits (ZMAS-3 [Mini-Circuits 2013]), which modulates the signal with BPSK modulation by alternating between a positive and negative voltage (in this case +/-5 V) at the control-port to generate a 180-degree phase shift of the output signal. Hence, the modulation can be controlled with a microcontroller and an additional voltage level converter to apply + or - 5 V. By having two Arduino Uno-boards (as presented in Section 3.2.2) pre-programmed, any switching of hardware at sea would be swift and also give a degree of redundancy if any of the two boards would fail. The complete back-up system is shown in Figure 3.10, and utilizes the same power distribution card, PA and a similar Arduino Uno microcontroller board as described in Section 3.2 for the transmitter.

3.6 Test Sequence

Custom programs were written for the Arduino Uno microcontroller boards (ref. Section 3.2.2) to control the Mini-Kits DDS and the back-up plan (Section 3.2.3 and 3.5 respectively). In general for both programs, the structure is to send out a known modulated sequence/package for several data rates, with a carrier sent out for approximately one second between each change of data rate. Each package contains a total of 50 bits. The first 20 bits are synchronization bits to make it

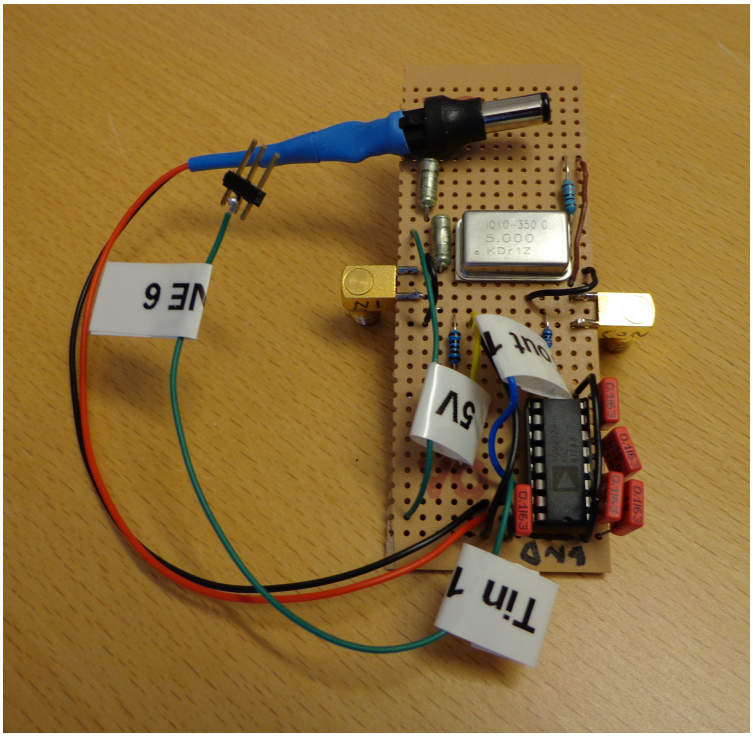

FIGURE 3.9: Back-up Circuitry Board.

detectable and makes it possible to determine which bits that are zeros and ones. The remaining 30 bits are data bits, which are individual for each of the different rates. Each with an equal number of zeros and ones to ensure an even amount of energy sent out for both symbols, and thus the assumption about equiprobability of the bits holds (ref. Section 2.4.4). To compensate for the duration of a bit sent with varying data rate, the packages transmitted with higher data rates are sent repeatedly to approximate the same energy per bit ratio (ref. Equation (2.23)) for comparison means as described in the Section 2.4.5 about repetition coding. The number of repetitions for the specific data rate corresponds roughly to the same time it takes to send one package with the lowest rate, in this case 237 bps for the primary hardware and roughly 200 bps for the back-up.

The program for the primary hardware, described in the following Section 3.6.1, also inherits a FSK modulated sequence in addition to the BPSK modulation. The FSK modulation is implemented in such a way that a carrier of 5.0 MHz and 5.1 MHz is transmitted for '0' and '1' respectively.

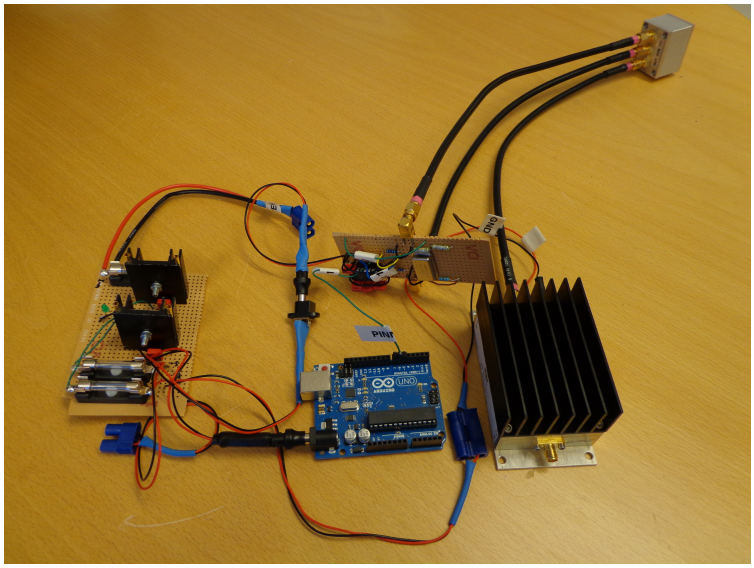

FIGURE 3.10: Back-up System Consisting of Power Supply Board, Arduino Uno Microcontroller Board, Back-up Board, ZMAS-3 BPSK Modulator (Northeast Corner) and RF Bay 1 W Power Amplifier.

3.6.1 Test Sequence - Primary Hardware

The Arduino code for controlling the DDS is given in Appendix A. In general, it consists of defining several control 'words' (each word consists of two to four bytes), and a main program that sends the words sequentially to the DDS in order to set different registers required to achieve desired functionality. In the beginning, several of these words are sent to set up registers in the DDS to get the desired output. E.g. the frequency control to get an sinusoidal output/carrier with the specified frequency. Afterwards, it enters an infinite while-loop, which sends out control words for the phase accumulator to get an BPSK modulation of the carrier. Several other delays and other control words are also sent out in order to get different data rates, bursts and delays as described in the previous Section 3.6. The data rates achievable are constrained by the Arduino Uno board for all practical purposes. Each time a new bit is to be sent, the microcontroller has to send out a program word to the DDS with a length of 32 and 16 bits for BPSK and FSK modulation respectively.

The communication between the two devices is limited by the speed of the communication protocol, serial peripheral interface (SPI) [Arduino 2013*b*], built in both boards. In this case a maximum of 4 MHz. In order to vary the data

rate and simplify the programming, the communication clock speed for the SPI is reduced to achieve a lower data rate. This may not be the optimal way of setting the data rate since it may not be a round number, but it is relatively easy and time efficient to implement. The resulting output data rates are approximately 237 bps, 825 bps, 11.641 kbps and 46.598 kbps for the BPSK-modulated data, and roughly 10 kbps for the BFSK. The largest bandwidth of the BPSK signals can then be calculated from Equation (2.30), using the highest data rate ($R \approx 46,700$ Hz):

$$BW_{BPSK} = 2 \cdot R = 2 \cdot 46,700 = 93.4 \text{ kHz} \tag{3.1}$$

For the BFSK case with a tone difference of 100 kHz, the formula 2.31 gives a bandwidth of:

$$BW_{FSK} = 2\Delta f + 2R = 2 \cdot 100,000 + 2 \cdot 10,000 = 220 \text{ kHz} \tag{3.2}$$

The sampling frequency of the Perseus SDR will then have to be larger than two times 220 kHz according to Equation (2.29). A sample of this test sequence recorded directly from the PA by the Perseus SDR is shown in Appendix D, Figure D.1 (A frequency offset discussed in the following Section 3.7 explains the sinusoidal envelope shown in the figure).

3.6.2 Test Sequence - Back-up Hardware

The code for the Arduino program is given in Appendix B. The structure of the program is basically the same as for the primary hardware solution in Section 3.6.1 above. Same type of packages is transmitted with 20 synchronization bits and 30 data bits. However, they are sent with 200 bps, 1 kbps and 114 kbps rate. A sample of the output is provided in Appendix D, Figure D.2 This time, the data rates are constrained by the speed of the microcontrollers ability to switch between 0 V and 5 V ('LOW' and 'HIGH' in the program respectively). This method is much simpler and time effective compared to what is required for the primary hardware, hence it makes it possible to achieve higher data rates.

3.7 BPSK Decoder

As mentioned in Section 2.4, to retrieve the data bits modulated into the carrier frequency of 5 MHz, the sampled waveform from the Perseus SDR receiver has to be demodulated and decoded properly. Due to the special output format from the Perseus SDR (discussed briefly in Section 3.2.3), a custom BPSK demodulator had to be implemented in MATLAB. The decoder program and an additional

check-program for validating the decoded data string are given in Appendix C. In general, the decoder exploits a small frequency offset, of roughly 42 to 44 Hz, between the Perseus SDR and the DDS, which reveals a sinusoidal envelope with the recorded frequency data modulated in it. Since the phase information of the sampled signal is recorded, a similar envelope should be possible to recreate by multiplying the data with a sine function in MATLAB, and then demodulate the new waveform. However, this is not needed since the small frequency deviation between the DDS and Perseus SDR already produces the desired waveform.

Several commercially available BPSK decoders for personal use can be found online. The MATLAB-code for the BPSK decoder used in this project is based on a code available on MATLAB Central [Ismail 2013], however it is heavily modified to fit into this specific application. This demodulator does not have any automatic synchronization or detection, hence it relies on several inputs from the user, such as defining starting point for the data burst, specifying data rate and also phase offset in order to synchronize the decoder properly.

This decoding structure is based on a technique where the recorded signal gets chopped up to blocks, on an incremental basis, into fractions with a size equal to the length of each symbol. Two similar sinusoidal waveforms, one sine and one cosine, with approximately same frequency are created in MATLAB and used as reference for comparison with the recorded signal. The best correlation between the sampled block and the reference sine/cosine determines if the bit is decided to be zero or one. This is much similar to the detection technique described in Section 2.4.5 concerning repetition codes. A plot from the decoder is given in Figure 3.11 where the sampled signal for three bits (green) is correlated against the reference curve for zeros (blue) and ones (red). The correlation is also showed in the same colors as the bits, whereas the magnitude away from the center indicates the degree of correlation.

A drawback of using this technique is that it relies on each symbol sent to be of constant size and a round number of samples. As the data rate gets high the number of samples per symbol gets low. In this case for the highest data rate of 46598 bps, a sample rate of 500 kSps yield approximately 10.73 bits per symbol. Thus, only a small offset in the incremental rate of chopping up the signal will lead to wrong samples being correlated after only a few iterations. A few small compensating measures has been taken to overcome this problem, but it only seems to track the right samples for roughly 170 bits for the highest data rate. This issue is mostly precarious for decoding high data rates, in this case the 11,641 and 46,598 bps. As a result of this synchronization issue, an assumption is made that as long as the first package (containing the same sequence of 50 bits as the rest of the sequence) is decoded correctly, the remaining packages could roughly be successfully decoded as well. Hence, only the first 50 bits of the sequence with the two highest data rates are decoded. Because of this, a BER

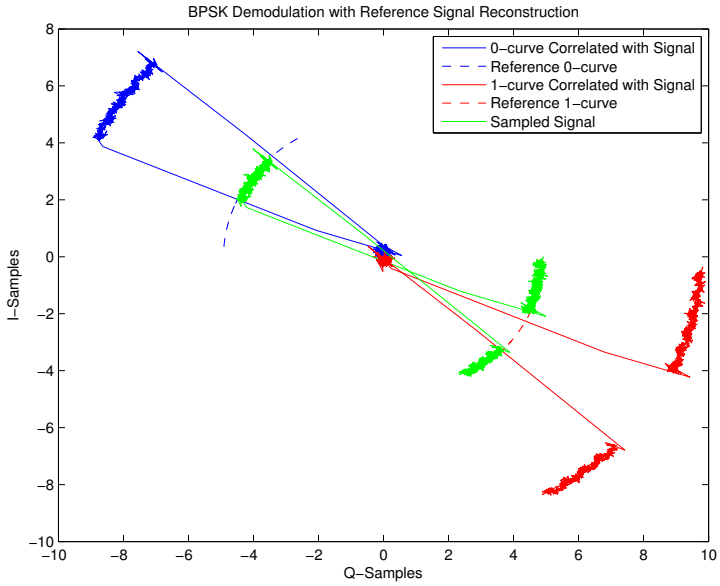

FIGURE 3.11: BPSK Carrier Reconstruction and Correlation of Symbols '1'-'0'-'1'.

analysis of the different rates is more or less useless. A more robust decoder with a better synchronization technique, such as with a phase locked loop, should be able to handle this offset better and be able to decode the rest of the packages properly. Thus, one can argue that the assumption can hold. Unfortunately, this synchronization issue also effects the decoding strategy described in Section 2.4.5. In theory, all of the bits in each package transmitted with the various data rates could be evaluated all together due to repetition of the packages. This would have increased the BER for the different data rates, and would also make them more comparable.

Due to time constraints, no decoder was developed to decode any output from the back-up hardware, nor for any FSK modulated signal. However, with small adjustments, the decoder described above should be able to decode the BPSK modulation from the back-up hardware since the waveform is roughly the same.

4

Measurements and Results

Two tests were conducted with the equipment in the seawater. Both tests were executed in a similar fashion even though the first was done on the boat R/V Gunnerus, and the other on a pier outside Trondheim Biological Station. Test procedures and results for the two tests are presented. Test one is given first, followed by test number two and at last results from the demodulation.

4.1 Sea Test I

4.1.1 Setup - Sea Test I

The first real test in seawater with the complete system was done on board of R/V Gunnerus, shown in Figure 4.1, Monday 22nd of April 2013. The R/V Gunnerus is a research vessel owned and operated by NTNU. The boat is heavily equipped with technological equipment such as dynamic positioning (DP), two cranes, wet- and dry-laboratories, etc. The DP system and cranes was especially helpful for this mission since it made it a lot easier to deploy the gear, and navigate steady towards the cNODE at the bottom.

A sketch of the measurement setup is given in Figure 4.2. The cNODE and one of the antennas were lowered down on the bottom by a large crane on the starboard side of the boat, and held vertically in the sea by a small buoy and 40 kg of weights down at the bottom. The cNODE should generally be held up from the bottom to ensure a reliable acoustic communication link. It was also desired to minimize any ground coupling for the EM waves propagated out from the antenna on top of the cNODE. A nylon rope was laid out about 50 meters along the bottom to avoid any tangling with the other antenna dragged after the boat. This rope was used to hoist the gear up and down in the sea. An additional battery-driven acoustic transducer for the Gunnerus own navigation system was connected to the rope close to the antenna. This helped the captain of the Gun-

FIGURE 4.1: R/V Gunnerus.

nerus to navigate close to the submerged gear. The other antenna with weights (30 kg), and our own acoustic transducer hung underneath, was lowered down in the water with another smaller crane on the port side of the boat (a photograph from the deployment is shown in Figure 4.3). This crane had an odometer integrated, which was used to adjust the depth of the gear. A similar battery-driven acoustic transducer was attached to the rope over the antenna for navigation purposes as mentioned previously in this section. Self-amalgamating/bonding rubber tape was used around the connectors of the cables between the submerged gear for insulation against any water penetrating into the connectors.

This first experiment was conducted outside Ranheim in Trondheimsfjorden, and the exact location is shown in Appendix E, Figure E.1. The location were chosen since it was in relatively good proximity to the dock where all of the equipment was loaded on board, and also due to low freshwater supply from surrounding rivers/creeks and stable sea currents. As can be seen from a mapping of the bottom in Figure 4.4, it is relatively flat at a depth close to 50 meters, which should give relatively equal effect on the results with respect to change in distance between the antennas. The cPAP system for the cNODE measured the range at an interval of approximately 1.53 seconds throughout the entire session, and also timestamped and logged the range automatically. A video recording from a digital camera was used to film the clocks of both the Perseus Software

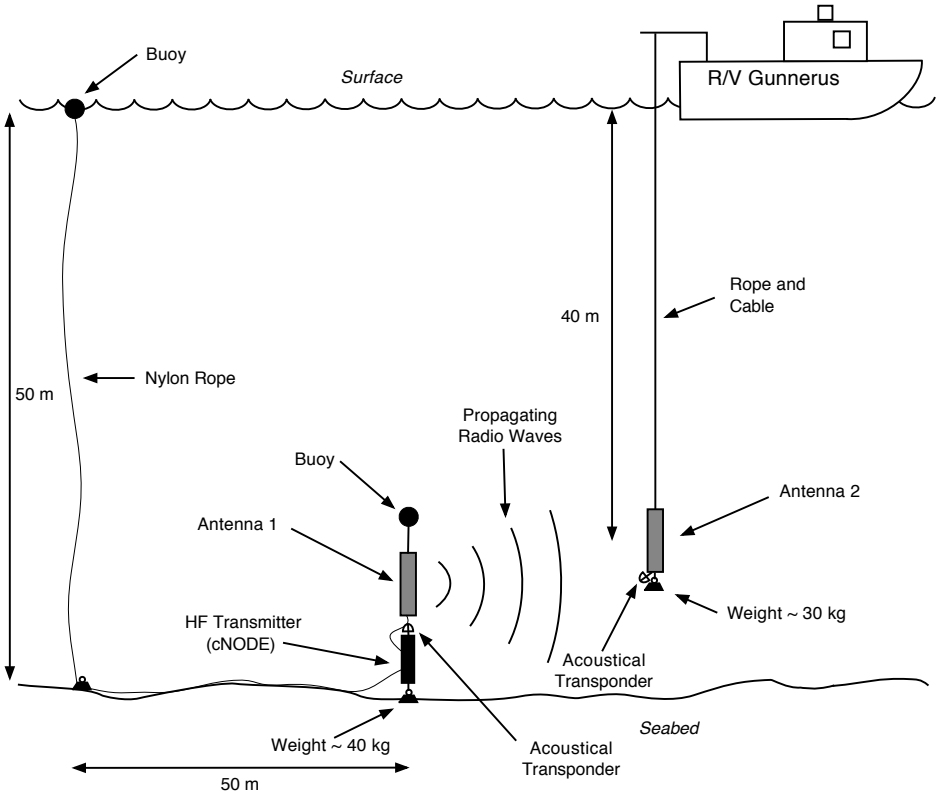

FIGURE 4.2: Measurement Setup Sea Test I.

and the cNODE-computer, and in addition a program providing a millisecond stopwatch. This was carried out in order to be able to synchronize the signal recordings with timestamps for the range log. The Perseus SDR Receiver was set up with a sampling rate of 500 kilosamples per second. This should be sufficient with respect to Equation (2.29), where the largest bandwidth of the transmitted signal was approximately 220 kHz (ref. Section 3.6.1). For a setup with 500 kSps, the Perseus SDR displayed effective bandwidth (visible bandwidth in the Perseus SW spectra) of 400 kHz and RBW of 488.3 kHz.

At the end of the trip, a conductivity, temperature and depth (CTD) probe was lowered down to the bottom. This retrieved information about the conductivity, salinity and temperature of the water versus depth at the same location. The results are presented in Figure 4.5 and shows that there only were

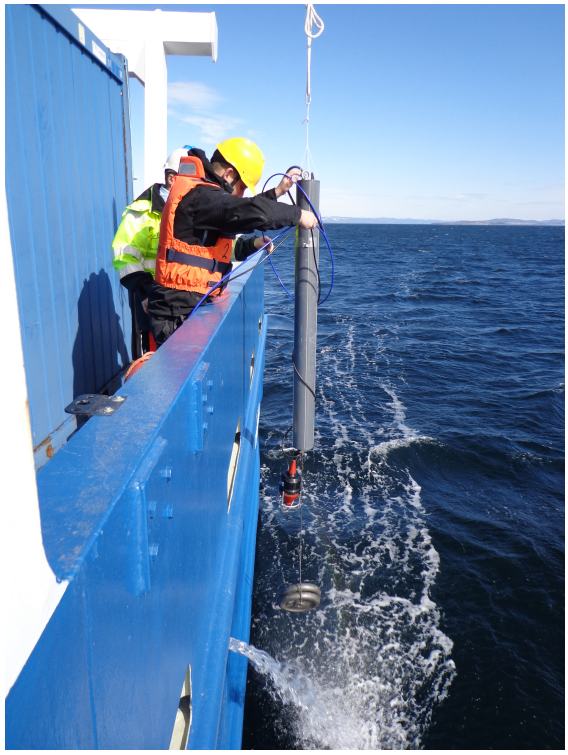

FIGURE 4.3: Measuring Antenna and Acoustic Transducer. Tore Landsem is Guiding the Equipment Down in the Seawater Outside Ranheim

small variations in all parameters throughout the vertical profile. Conductivity and salinity varies from roughly 3.15 to 3.33 and 32.6 to 33.6 respectively. Notice the small but abrupt increase around 11 to 15 meters. This could indicate a junction due to a layer with a larger amount of freshwater.

4.1.2 Results - Sea Test I

The recorded results from this test were more or less discouraging. There was no signal detected at all, even with a minimum measured distance of roughly 2 meters. After the equipment were hoisted up, seawater was discovered in one of the N-connectors linking the coaxial cable from the Perseus SDR with the antenna dragged from the boat. The effect of seawater in the connector (with

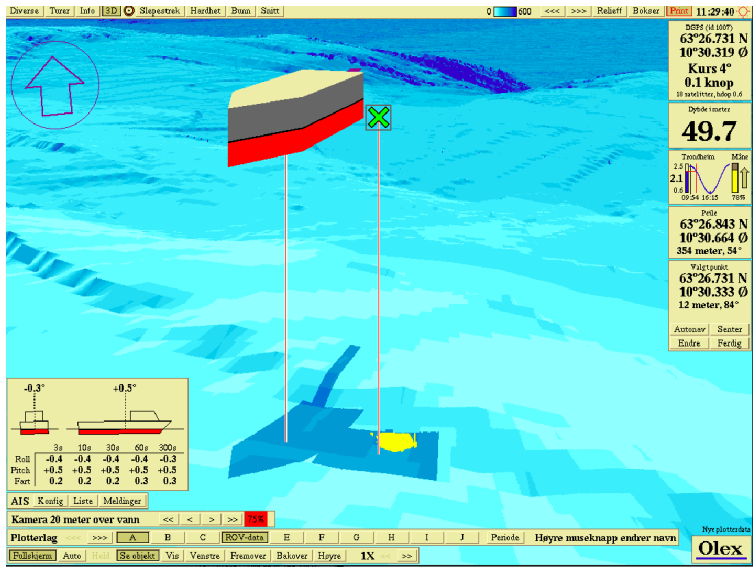

FIGURE 4.4: Location and Depth Profile from Ranheimsbukta April 22nd, 2013. From the Gunnerus own OLEX Ocean Mapping System.

the antennas in air) was measured to be roughly 20 dB loss of signal strength.

4.2 Sea Test II

4.2.1 Setup - Sea Test II

Due to the absent results from the first test, a second field test was conducted on the pier at Trondheim Biological Station (TBS) the 30th of April, 2013. A map with coordinates is given in Appendix E, Figure E.2. This location is believed to be more susceptible for freshwater mixing from the large river, Nidelven, which has its outlet a few hundred meters down south from TBS. Conductivity of the water is thus assumed to be somewhat different than in Figure 4.5. The setup was approximately the same as in the previous Sea Test 1 (ref. Figure 3.1), besides that the depth at that location was measured manually to be roughly 11 meters and not 50 meters as in the first test. This depth was considered to be sufficient to avoid any possible propagation path through air as well. Due to the proximity to land, the depth profile where not flat but tilted upwards the shore

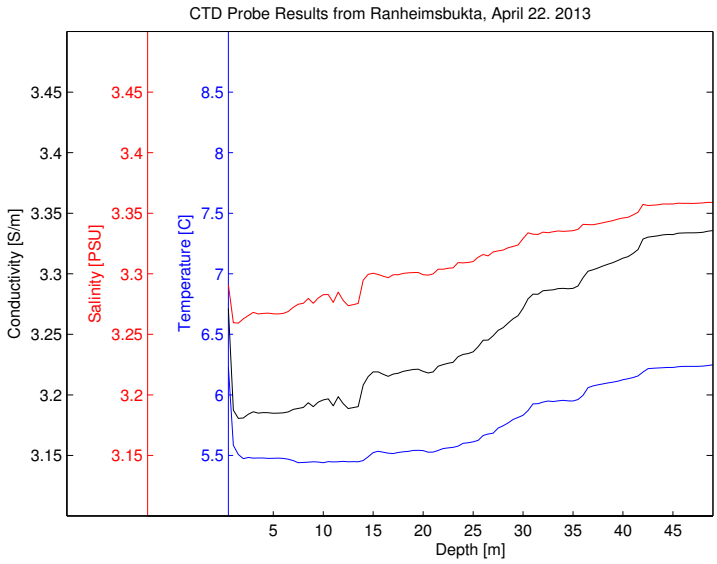

FIGURE 4.5: CTD Profile from Test Location I April 22nd, 2013.

and containing solid bedrock. The acoustic transducer was also placed on top of the antenna, as opposed to the first test. An on-site crane was used to lower down the cNODE and on of the antennas, and afterwards to navigate the other antenna around for measurements. This crane allowed us to have good control of the range between the antennas at all times, however, it was not so easy to control that both antennas were at equal depths, as desired (ref. Section 3.4), throughout the session.

In this test, the FSK functionality of the modulator was turned off, in belief of that the FSK modulation of the carrier would complicate the decoding of the BPSK-modulated data. At that time the decoder described in Section 3.7 was not finished, thus a decision was made to just use BPSK modulation in order to save time decoding the data afterwards. In recent time, this turned out to be a wrong assumption.

4.2.2 Results - Sea Test II

Since the depth was significantly shorter along with the use of a crane, it was possible to navigate the antennas almost directly next to each other. The graph in Figure 4.6 shows a boxplot of the measurements from the whole test. Four tests were conducted with somewhat inconsistent results. The boxplot shows both median and variance of the four datasets combined. The blue boxes represent 25- and 75 quantiles of all the data points in each group. The red line is the median for the specific group, whilst the black bars on top and bottom represents the remaining data points not regarded as 'outliers', which are the red crosses. A few range measurements was extremely larger than others at the roughly the same time interval, in the order of tenths of meters, and those samples was assumed to be un-valid and thus discarded from the data set. As can be seen from

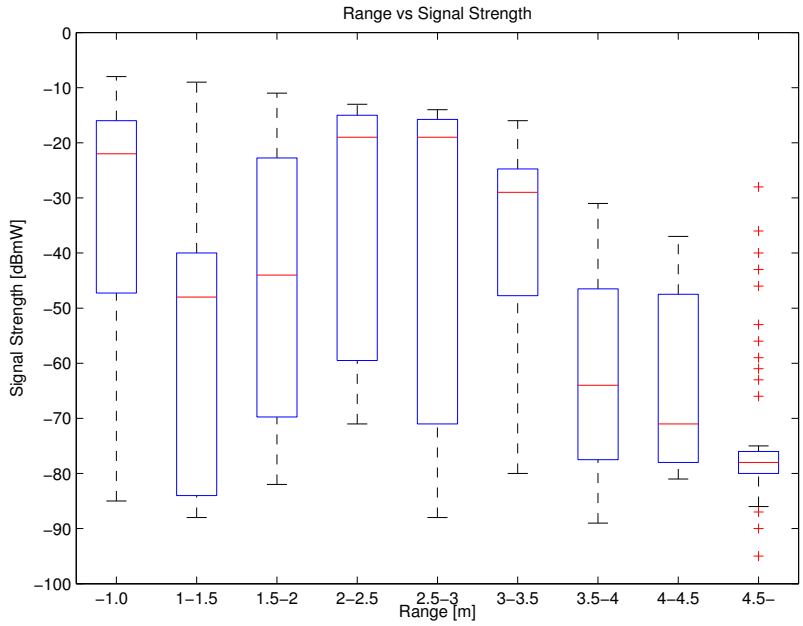

FIGURE 4.6: Measurement Results Outside Trondheim Biological Station
Depth Approximately 11 meters, 206 Sampled Values.

the figure, the results are quite varying. However, the trend shows decent signal strength within roughly 3.5 meters, after that it seems to go decrease drastically. At approximately 5 meters the signal strength is in overall close to the noise level

measured at roughly -110 dBm.

One of the measurements was done with the acoustical transducer underneath the antenna instead of on top as described in the previous section. In general for that specific test, the received signal strength was relatively weak, and most of them are represented in the lower section in Figure 4.6.

A small surprise was the AM radio signals could be detected close to the surface, indicating that EM waves do cross the air-water interface.

4.3 Decoding the Results

The waveform shape of the recorded signals is given below in Figure 4.7. The waveform shows a clear BPSK modulation similar to the sample from Figure 2.8. As long as the received signal level is strong, the waveform shape seems to be relatively nice and clean. At least for the short period of time the shown waveform represent. With the custom made decoder described in Section 3.7, the

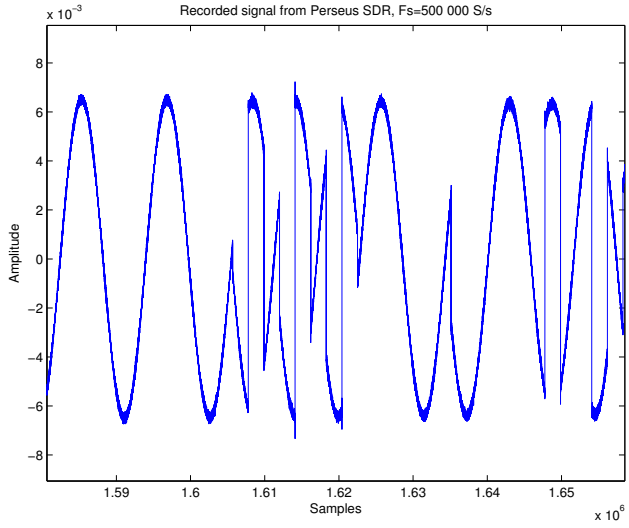

FIGURE 4.7: Measured BPSK Modulated Waveform with Signal Strength of -38 dBm. Modulation Rate = 237 bps.

correct data bits can be extracted from the waveform as long as the signal level is strong enough for a given data rate. A table of the results from the decoding is presented in Table 4.1. The SNR is found by a visual read-out of the Perseus

SW at the corresponding time for the decoded signal sequence. Notice the high

TABLE 4.1: Decoded Number of Bits from Sea Test II.

Data Rate	**# of Bits Decoded**	**Signal Strength**	**SNR**
237 bps	50 bits	-72 dBm	38 dB
825 bps	150 bits	-60 dBm	50 dB
11641 bps	50 bits	-48 dBm	62 dB
46598 bps	50 bits	-40 dBm	70 dB

SNR required. E.g. 50 dB for 825 bps data rate. The reason is believed to be because of the manual detection and synchronization of the received signal for demodulation. These SNR levels should have been possible to improved by using more time in the manual decoding work and a more robust structure in the decoder program.

5 Discussion

At first a discussion of the results followed by a section regarding measurement uncertainties and difficulties for the two test comes first. The measured results are compared afterwards to theoretical values and also results from other researchers, followed by a round up of the channel capacity and attributes. At last the performance of both hardware and decoder is evaluated.

5.1 Sea Test I

5.1.1 Sea Test I - Results

The results from the first test were, as mentioned, nothing to cheer about. No signal was detected at all, even at the smallest range at about 2 meters. It is believed to be mostly due to the water having penetrated through the insulation and into the coaxial connectors of the antenna dragged after the boat. Although only roughly 20 dB increased loss was measured back at the lab with seawater in the connectors, there is a possibility that the additional loss could be different with the gear fully submerged in seawater.

Another potential source of signal loss can be the acoustic transducer that was hanging below the same antenna. This cable hung right next to the antenna, and may have suppressed some of the performance of the antenna by inducing EM coupling. The effect of the acoustic transducer hanging below versus on top of the antenna was tested out in the second test, and the results of this is discussed more thoroughly in Section 5.2 concerning the results from test two.

5.1.2 Sea Test I - Measurement Uncertainties and Difficulties

Even though R/V Gunnerus had DP, it was not easy to come any closer than approximately two meters with the antennas. The separate acoustical transducers provided from R/V Gunnerus was mounted on both the rope connected to the antenna on the bottom, and also on the other antenna dragged after the boat to make the navigation easier for the captain. These were however attached to the nylon rope laying out on the sea floor roughly one meter from the antenna, which in turn might gave a small offset on the navigation system with respect to the actual placement of the gear. Also the depth of the second antenna hanging from the boat could have been monitored more closely to further decrease the distance between the antennas. The depth of this antenna was adjusted briefly during the test, but due to a large time pressure on completing the test, this depth was probably not as optimal as it could have been.

5.2 Sea Test II

5.2.1 Sea Test 2 - Results

The second test gave promising results. Even though the variance in signal levels versus range seems to be quite large (ref. Figure 4.6), they show that it is possible to get a reasonable signal level within a few meters. Based on Table 4.1 showing actual decoded bits, at least a rate of 237 bps should be achievable for roughly 3.5 to 4 meters. A transmission with the highest data rate in this test of 46598 bps could be as long as 3 to 3.5 meters according to these results. The depth of the submerged antennas was approximately 9 meters. A signal path from water, up in the air, and down through water again is assumed to be negligible/non-present since the geometrical distance is at least twice the depth (18 m) and significantly larger than the maximum range recorded of 5 m.

5.2.2 Sea Test II - Measurement Uncertainties and Difficulties

The measured signal strength versus range seems to be somewhat inconsistent. A potential source of this high variance can be the synchronization between the clocks of the Perseus and cNODE-computer. As described in Section 4.1.1, a camera was supposed to document the offsets of the recordings with respect to

the logged ranges. However, after closer inspection it turned out that the cNODE computer and the program logging ranges did not use the same internal clock. This was not discovered until after the testing was done. After some examination of the timestamps of the files containing the ranges, the offset was found to be approximately 59 minutes and 72.7 seconds. This was corrected from the range log, but the offset could be smaller or larger if the timestamps where not exactly accurate. By correlating the measured signal levels with the range log, it should have given a clue about the clock-corrections to be either too high or too low. This visual correlation turned out to be very ambiguous, since some data indicated the corrections to be too low, while others inferred the opposite. Thus, the offset mentioned was assumed to be as accurate as possible.

All except one of the measurements this second test was carried out with the acoustic transducer on top of the antenna as opposed to underneath. The range measured with the acoustic system would then give an geometrical offset of at least the length of the antennas (1.52 m) when they where exactly next to each other. This offset was corrected by simple geometrical calculations. However, the calculation where based on the antennas being at exact equal depths, which could not be guaranteed at all times. It is apparent that the antenna from the crane was sometimes a bit lower than the antenna connected to the cNODE, because of the uncalibrated ranges sometimes was less than 1.5 meters. Since there was no apparent way to estimate the vertical offset, the calibrated ranges are assumed to be in ballpark accurate, and sort under their respective groups in Figure 4.6. This problem could be handled better with a more thorough systematic testing and documentation. The crane standing on the pier did not have any odometer either, which would have made it easier to control the depth of the measuring antenna.

Another aspect of having the acoustic transducer underneath is that it seems to give some effect on the measured values. In general, there was detected lower signal strength in the measurement with the transducer underneath the antenna compared to above. There is a chance that the cable connected to the transducer induced a variation in the characteristics of the antenna. This could make the antenna perform worse, and also be one of the reasons for not receiving any signal in Sea Test I. In addition, the bottom was not flat as mentioned in Section 4.2.1. If the solid bedrock lies very close to the gear, then this could effect the EM signals and maybe improve the results. A test of this effect was done in Fjuk [2012], but no such thing was measured for that specific seabed material.

5.3 Measured Results vs. Theory

By combining the boxplot of the measurement results presented in the preceding Section 4.2.2 with a graphical representation of the link budget Equation (2.19), a visual comparison can be made. The parameters for the link budget equation are relatively the same as the specifications of the equipment used in the actual tests and are listed in Table 5.1. Since we did not have a CTD-probe available during this test, the conductivity is varied between 2 S, 3.2 S (the same as in Sea Test I) and 4 S. 3.2 S should be regarded to be the highest possible conductivity for this specific case since that was the value measured in Sea Test II. However, this second test location is relatively close to the outlet of Nidelven as pointed out in Section 4.2.1 and thus a higher degree of freshwater mixing is probable to have occurred. The actual conductivity is hence more likely somewhat smaller than 3.2 S. The loss through 100 meter of coaxial cable connecting the antenna

Table 5.1: Link Budget Parameters.

Description	**Parameter**	**Value**
Transmitted Power	P_{TX}	+30 dBm
Antenna Gain	G	-5 dBi
Antenna Reflection Loss	$\left(1 - \lvert\Gamma\rvert^2\right)$	-5 dB
Range	R	0 to 5 m
Wavelength	λ_r	7.07 m
Cable Loss	L_a	2.36 dB
Relative Conductivity	σ_r	3.2 S
Relative Permittivity	ε_r	72

dragged after the boat and to the Perseus SDR Receiver is also accounted for in the term for additional loss L_a. The gain G and reflection loss $\left(1 - \lvert\Gamma\rvert^2\right)$ of the antennas are the two parameters that are hardest to estimate. The antenna gain will not be as good as for an ideal dipole antenna due to its wideband characteristics, and since it is not a half-wave dipole. As described in Fjuk [2012], both the resistance and length of the antenna is lower than ideal for operating at 5 MHz. In addition, not all the power fed to the antenna is radiated out, but also dissipated as heat from the ohmic resistance of the antenna [Balanis 2005, p. 80]. Because of this, a gain of -5 dBi is estimated for both antennas. A measurement of the transmission characteristics of the antennas revealed a larger loss than

experienced when they were made and tested half a year ago [Fjuk 2012]. There has apparently been some deterioration of the antennas in this period of time. A comparison of tests from a network analyzer yielded substantial differences in performance over the frequency band of interest over this period of time. The most probable cause is water that has penetrated the isolation around the feeding point of the antennas and reacted with the copper line of the coaxial feed, resulting in corrosion. An endoscope was inserted into the PVC-tubing capsuling the antenna to investigate if there was much corrosion of the metal in the antenna. Only the large cones of brass were visible, but that section seemed to be fine. Hence, either the copper of the feeding line or maybe the welding done on the antennas are the most probable cause of any deterioration and increased loss. A reflection loss of -5 dB is estimated since the antennas are not exactly matched to 50 ohms [Fjuk 2012], and because of the deterioration mentioned previously.

The resulting link budget and the boxplot with results are provided in the next Figure 5.1. The theoretical loss seems to be a bit larger than experienced,

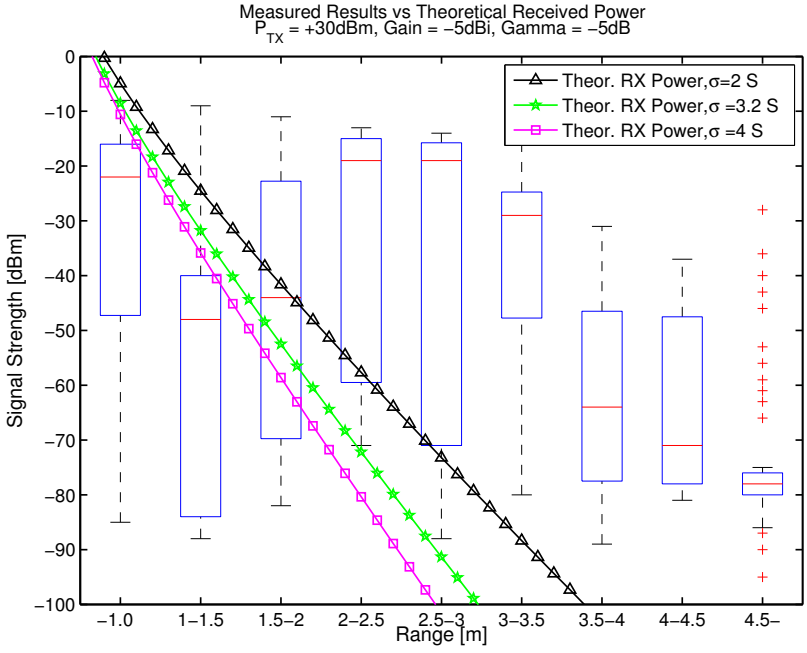

FIGURE 5.1: Measured vs. Theoretical Received Power.

even though it is not by much. By the theory presented in Section 2.2 and the parameters in Table 5.1, the range should theoretically not have exceeded roughly

3 meters before it goes below -100 dBm. However, the measurements done in this second test gave a maximum range closer to 5 meters at best. If the output power of +30 dBm and conductivity 3.2 S is used as a reference, the signal with attenuates to -100 dBm after 3 m and 5m for theoretical and actual range. This yields an attenuation of approximately -43.3 and 26 dB per meter respectively.

The actual effect of all the previously mentioned uncertainties is hard to estimate, and the actual difference between real life- and theoretical performance might be smaller. Especially since the conductivity parameter is highly questionable. It is probably in the lower region somewhere around the 2 S plot for these specific measured, but for subsea environments it should be close to 4 S, (ref. Section 2.2). As mentioned, the CTD measurement in Figure 4.5 showed most variations from approximately 11 to 15 meter. This is believed to come from a freshwater junction. Since the outlet from Nidelven is close by, this freshwater-seawater layering effect may thus be larger in this area. If the measurements were done in a freshwater junction, then this would maybe explain some of the large variations in the results.

As mentioned briefly in Section 4.2.1, the depth profile was not exactly flat. Bedrock close by could have affected the measured power levels positively and hence explain some of the additional range experienced. Even though no such effect was observed in the previous project measurements [Fjuk 2012], it cannot be ruled out since the seabed conditions at that place was unknown.

With the conductivity discussion in mind, and the non-appearing signal in Sea Test I. Given that the conductivity parameter in the second test is significantly lower than estimated and hence explains the relatively lower attenuation, a high conductivity in the order of 3.2 S would give the presented theoretical attenuation in Figure 5.1. This would at maximum give a maximal range up to roughly 3.5 m. Adding further loss from seawater in the connector and possible negative influence from the cable connected to the acoustic transducer hanging below the antenna, the theoretical range is reduced further. Combining all of these three sources of signal loss could result in a higher attenuation and explain that there was no signal recorded at the minimum range of approximately two meters. If the range between the antennas could have been minimized further, then there is probable that a small signal would have been detected eventually.

As inferred from Section 1.2 and 2.1.3, concerning previous results and medium range phenomena respectively, none of these effects is observed in this thesis. Since the measured range is in ballpark the same as in theory, it is reason to believe that there actually was a current flowing on the outer conductor as described in Section 1.2. For the case of medium range phenomena, the Perseus SDR did not measure as low as down to -120 dBm as shown in Figure 2.1 for the results presented by Shaw [2006]. By comparison with our own results from Figure 4.6, the large attenuation in the beginning is similar, except that our sig-

nal drops down into the noise floor. It is of course possible that the phenomenon was present, but it could not be visible in our data. It did not appear on the portable spectrum analyzer either, even though the noise floor was a bit lower for that apparatus.

5.4 Channel Capacity and Attributes

This project has proved that an modulated EM-wave can be successfully transmitted and received through seawater. From Figure 4.7, seawater seems to be relatively linear in the time domain as a communication channel for a small frequency band. The variation should be larger over a wider frequency span according to theory. Both the dielectric loss tangent described in Section 2.2.2 and the skin depth from Section 2.2.3 shows a large variation in the attenuation constant around the lower MHz-domain. Actual measurements from previous work (ref. Fjuk [2012]) also support this statement. However, the degree and effect in phase and/or amplitude of this variation are difficult to estimate.

Due to the high attenuation of the EM signals through the water, a small decrease in range gives a relatively high increase of the SNR. Just by reducing the range from four to three meters seem to give up to 40 dB increased signal strength according to Figure 4.6. This means that variations of phase and amplitude versus frequency may not be as important if a high SNR can be achieved with small adjustments in the range. Figure 2.12 displaying Shannon's capacity theorem in Section 2.4.7 yields an theoretical upper limit of several megabits for relatively small bandwidths in the order of a few hundred kilohertz. Thus, a narrow band signal should achieve a high data rate by utilizing complex modulation schemes and channel coding. In addition, several frequency channels with a few kilohertz bandwidth can be used in parallel to transmit even more information if necessary. Since the attenuation is as high as it is, any interference with nearby transmitters should not be very problematic. Thus, a single user for transmission can use most parts of the EM spectrum.

5.5 Hardware Performance

In general, the hardware performed satisfyingly. The transmitter turned on successfully after acoustically controlled power-up a multiple of times, and both the 1 A fuses and voltage regulators could handle all the power that was necessary. The whole system consumed approximately 8.5 W during transmission and dissipated at least 7.5 W into heat. Even though this seems to be relatively small,

tiny droplets of condensated water could be found inside the cNODE top section module. By a visual inspection of the water absorbing salt (ref. Section 3.2.4), only a couple of very small dots indicated any water absorbed. These watermarks could easily have been made when opening the cNODE to disconnect the power after the tests. Thus, the small power consumption did not create any substantial condensation. This could however be a problem if a larger PA is used later on.

Another issue worth mentioning is the Arduino Uno microcontroller board. The EME165 DDS board did not require a lot of pins for this minimal application, but it could require 14 pins for maximum usage. The Arduino board has only 14 digital pins, so there is not much overhead for any expansion etc. The microcontroller also seemed to be a bit unstable in some sense. By monitoring the output signal, it looked like some of the transmitted packages were interrupted. Possibly because of some timer overflow or similar effects. It did not give any large problem while running, but it should be taken into consideration in designing a new software program.

Both the sampling frequency of the Perseus and range-measuring interval could be increased to get more precise data. The maximum sampling frequency of the Perseus is approximately 2000 kSps. This would have increased the effective bandwidth from 400 kHz to 1600 kHz, and thus also the noise power resulting in a lower resolution. The amount of data would also be substantially higher (2.3 GB for 5 minutes with 2000 kSps vs. 660 MB for 15 minutes with 500 kSps), which could add complexity for the decoding SW. The range measuring interval could be set down to 0.8 seconds at minimum. This would have given almost twice as many data points and perhaps less variance in the measured ranges.

The entire transmitter and the two antennas could be significantly decreased in size. This system requires a lot of space and weight in order to be wideband and versatile. For a frequency specific application the power distribution, microcontroller, DDS and PA could be combined onto only one circuit board with a fewer components. The antennas could also be minimized further to get a more compact design that would fit better on an ROV or subsea installation as inferred in Section 1.1.

5.6 Decoder Performance

The decoder performs suboptimal for the most cases. Because of the issues described in Section 3.7, it does not perform well over time due to synchronization issues. When the decoder drifts off and gives a wrong output, the following symbols also gets interpreted wrong. As of this reason, it is hard to estimate the BER for the different rates. As per now, this decoder system requires several inputs from the user in order to function properly. For signals with a low SNR, it can

be difficult to interpret and find the inputs needed. This adds complexity and uncertainties in the decoding, and thus lowering the performance for low SNR. As mentioned under Table 4.1, the SNR needed for decoding is relatively large. This problem could have been easier to handle if there were used a better communication protocol and relaxed synchronization requirements for the decoder.

In order to improve the decoding a better decoder with automatic synchronization such as phase locked loop should be implemented. The signal might also be easier to decode if the actual power levels was recorded instead of the frequency data (ref. Section 3.3.1) as from the Perseus SDR.

6

Concluding Remarks

Electromagnetic digital communication at 5 MHz through seawater has been proved to be possible. At least a data rate of 46 kbps is possible to achieve within a few meters of range. Due to the high conductivity, the signal attenuation is very high and thus the range is relatively low compared to EM communication through air. Theoretical attenuation of the signal at 5 MHz is 43.3 dB per meter in seawater conditions such as in Trondheimsfjorden. In the actual measurements from Sea Test II, the maximum range was measured to be roughly 5 m outside TBS at a depth of approximately 9 meters. Although, the conductivity at that specific location is most likely to be somewhat lower due to proximity of the river Nidelven, which supplies freshwater into the seawater and hence increasing the range. The depth profile at the test location is also questionable with respect to possible interference from the adjacent bedrock. Since the transmitter was independent and battery driven, the signal received is guaranteed to have been propagated through seawater. Hence no signal leakages from cables or similar could have effected the measured values. Because of the poor quality of the antennas, the actual radiated power was probably significantly lower than the +30 dBm from the PA, giving a shorter range than possible with the same output power.

Although the concept has been proven, very limited knowledge of the field is still available and should be investigated. Comprehensive testing with more optimized equipment is required to gather a deeper and more detailed understanding of underwater EM communication. Similar tests as with R/V Gunnerus in Sea Test I should be repeated since the depth and seabed conditions can be monitored precisely. Several improvements of this specific system ought to be considered before further testing. A more compact antenna and transmitter/transceiver design is discussed in the next chapter, along with proposed changes regarding tests of more advanced digital communication.

7 Future Work

7.1 Optimized Antenna

The two antennas used in this project are quite large and heavy. Main reason for this is the use of freshwater inside the PVC-encapsulation. This is a design recommended from Yip et al. [2008], however the effect of this freshwater is relatively uncertain. Therefore, more ordinary and compact antennas may not give a large difference in performance and thus be a better option. A smaller and lighter design should be designed and fabricated to be more applicable for use on both a movable ROV and permanent subsea installation integration. A commonly used monopole could be used (usually referred to as a "whip" type), which is a small and compact antenna. It is basically just a vertical wire, preferably on top of a large metal sheet, such as on car roofs for traditional AM and FM radio broadcasts, and do not necessarily have to be very large. A fraction of the wavelength could be enough [Balanis 2005, p. 186]. The wavelength for 5 MHz is given below in Equation (7.1):

$$\lambda_r = \frac{\lambda_0}{\sqrt{\varepsilon_r}} = \frac{c/f}{\sqrt{\varepsilon_r}} = \frac{300 \cdot 10^6/5 \cdot 10^6}{\sqrt{72}} = 7.07 \text{ [m]} \tag{7.1}$$

Another small antenna type, the loop antenna can also be effective for this application. A small loop antenna has a loop with the circumference in the order about one tenth of the wavelength [Balanis 2005, p. 231] which is about 70 cm in this specific case. The corresponding diameter is roughly 22 cm. Recall the discussion about the company WFS Technologies in Section 2.1.4, they also use loop antennas heavily in their products.

7.2 Transceiver System

For general testing, the transmitter in Section 3.2 should suffice. Higher orders of PSK and FSK modulation types is easy to implement with just a few lines of code, given some experience with the DDS architecture and programming. To achieve a higher data rate, the microcontroller has to be switched with a better microcontroller that master a higher SPI-communication rate.

On the receiver side, another SDR radio that records the signal strength directly might be more appropriate. This would ease the demodulation process, since it does not demand to be re-modulated again as it has to be now. Live decoding could also be useful for field-testing purposes. Then the BER could be measured directly at specific distances, and it would also relax the amount of post-processing the data. A modulation scheme that does not demand coherent detection, such as FSK, could be a wise choice. Such a scheme would increase the bit error probability (ref. Figure 2.11), but simple channel coding could improve this. SW for demodulating the signals is of course required. Either by already available demodulator programs or in worst case a custom made program.

As mentioned in both the discussion and conclusion, the size of the HW could be decreased significantly. About all of the hardware could be fitted on one circuit board, and in addition a receiver also. This would be very interesting to in a ROV/subsea installation integration point of view. Higher output power could also be used, however this would also increase the power dissipated into heat and possibly create condensation issues.

7.3 Testing

Our experience from the two test conducted in this thesis gave a lot of experience of field-testing. The main issue in both tests was the time constraint. The time available on the boat was only a few hours since there were others that had booked R/V Gunnerus in the first place. The second test outside TBS was during the evening, thus the descending dawn was the main concern here. Even though we managed to perform the tests, it would definitely have been an advantage of having more time. Then it would have been easier to overlook the preparations and testing itself to assure it was conducted the right way and documented properly.

A more thorough test of the EM properties of seawater should be conducted to gather more information of the channel. Information regarding the phase response of the seawater should be investigated more thoroughly. A test with two antennas connected to a network analyzer would yield the phase vs.

frequency response. This would be of great interest for applications that requires a large bandwidth. In case of any large nonlinear effects, smaller and several channels could be used to mitigate this effect. A similar test was conducted in the preceding project, but because of some settings in the network analyzer this information was not stored. A similar setup as in the first test, Sea Test I, would give a better control of depth and seabed conditions. EM parameters such as the conductivity would also approach more to subsea conditions compared to in Sea Test II.

Another helpful aid to synchronize the clocks would be to utilize the automatic logging feature of the cPAP system better. All commands given from the cPAP-computer to the cNODE is logged automatically. E.g. power-up of the hardware, range logging etc. These functions could have been used more systematically when recording with the Perseus SDR receiver. Either the HW or range logging could have been started up at the same time recording is initiated.

Appendices

A

Primary DDS Program

```
/*  Primary Program with BPSK and FSK
    For Arduino Uno and Mini-Kits EME165
    Chip Select (CS) is always grounded
    IO UPDATE and IOSYNC is equivalent on the EME165-board layout design
*/\\

//-----Declarations-----//\\
\# include <SPI.h>\\

//--Pins\\
int RESET = 4;       // Reset pin, normally LOW\\
int SPI\_SCK = 13;    // Serial Clock \\
int SPI\_MISO = 12;   // Master In Slave Out\\
int SPI\_MOSI = 11;   // Master Out Slave In\\
int SPI\_SS = 10;     // Slave Select pin\\
int IOUPDATE = 5;    // I/O Update pin\\

//--AD9954 DDS Registers\\
byte CFR1\_adr = 0B00000000;  // Control Function Register No.1 (0x00) - 4
     Instruction bytes\\
byte CFR2\_adr = 0B00000001;  // Control Function Register No.2 (0x01) - 3
     Instruction bytes\\
byte ASF\_adr  = 0B00000010;  // Amplitude Scale Factor Register (0x02) - 2
     Instruction bytes\\
byte ARR\_adr  = 0B00000011;  // Amplitude Ramp Rate Register (0x03) - 1
     Instruction byte\\
byte FTW0\_adr = 0B00000100;  // Frequency Tuning Word 0 (0x04) - 4
     Instruction bytes\\
byte POW0\_adr = 0B00000101;  // Phase Offset Word 0 (0x05) - 2 Instruction
     bytes\\
byte FTW1\_adr = 0B00000110;  // Frequency Tuning Word 1 (0x06) - 4
     Instruction bytes\\
byte NLSCW\_adr= 0B00000111;  // Negative Linear Sweep Control Word (0x07) - 4
      Instruction bytes\\
byte PLSCW\_adr= 0B00001000;  // Positive Linear Sweep Control Word (0x08) - 4
      Instruction bytes\\\\

// RAM Segment Control Words, active when Linear Sweep is disabled\\
byte RSCW0\_adr= 0B00000111;  // RAM Segment Control Word 0 (0x07)\\
byte RSCW1\_adr= 0B00001000;  // RAM Segment Control Word 1 (0x08)\\
byte RSCW2\_adr= 0B00001001;  // RAM Segment Control Word 2 (0x09)\\
byte RSCW3\_adr= 0B00001010;  // RAM Segment Control Word 3 (0x0A)\\

// Frequency Tuning Word for 5.0 MHz\\
int FTW0\_5MHz[4] = {  // 0x03 33 33 33 \\
  B00000011,    //b3\\
```

```
    B00110011,     //b2\\
39  B00110011,     //b1\\
    B00110011,     //b0\\
41  \};\\
    // Frequency Tuning Word for 5.1 MHz\\
43  int FTW0\_5\_1MHz[4] = {  // 0x03 43 95 81\\
    B00000011,     //b3\\
45  B01000011,     //b2\\
    B10010101,     //b1\\
47  B10000001,     //b0\\
    \};\\
49
    // Phase Offset Word for 90 degree phase offset between each sample\\
51  //  Phase offset = (Deg/360)*2\^14 \\
    int POW0\_0deg[2] = {  // 0x10 00   90 degree Offset: --> 4096 Dec = 1000 Hex
        \\
53  0B00000000,     //b1\\
    0B00000000,     //b0\\
55  \};\\
    int POW0\_90deg[2] = {  // 0x10 00   90 degree Offset: --> 4096 Dec = 1000 Hex
        \\
57  0B00010000,     //b1\\
    \};\\
59  int POW0\_180deg[2] = {  // 0x10 00   180 degree Offset: --> 8192 Dec = 2000
        Hex\\
    0B00100000,     //b1\\
61  0B00000000,     //b0\\
    \};\\
63  int POW0\_270deg[2] = {  // 0x10 00   180 degree Offset: --> 12288 Dec = 3000
        Hex\\
    0B00110000,     //b1\\
65  0B00000000,     //b0\\
    \};\\
67  int POW0\_360deg[2] = {  // 0x10 00   180 degree Offset: --> 16384 Dec = 4000
        Hex\\
    0B00100001,     //b1\\
69  0B11111111,     //b0\\
    \};\\
71
    void setup()\{\\
73  //Declare pins as output and set low\\
    pinMode(RESET, OUTPUT); \\
75  digitalWrite(RESET, LOW);\\
    pinMode(SPI\_SCK, OUTPUT);\\
77  digitalWrite(SPI\_SCK, LOW);\\
    pinMode(SPI\_MOSI, OUTPUT);\\
79  digitalWrite(SPI\_MOSI, LOW);\\
    pinMode(SPI\_MISO, INPUT);\\
81  digitalWrite(SPI\_MISO, LOW);\\
    pinMode(SPI\_SS, OUTPUT);\\
83  digitalWrite(SPI\_SS, LOW);\\
    pinMode(IOUPDATE, OUTPUT);\\
85  digitalWrite(IOUPDATE, LOW);\\

87  //Initialize SPI communication\\
    SPI.begin();\\
89  SPI.setBitOrder(MSBFIRST);  // Set SPI to send MSB first\\
    SPI.setDataMode(SPI\_MODE3);  // Clock is idle HIGH, and data shifted in on
        rising edge (1, 1)\\
91  SPI.setClockDivider(SPI\_CLOCK\_DIV4);  // 1/4 of the clock frequency
        \{2,4,8,16,32,64,128\}\\
```

```
}\\
93
void loop()\{\\
95
  initDDS();   // Set up DDS to have carrier of 5 MHz\\
97  delay(1000);  //Delay in milliseconds\\

99  //--Test sequences containing 50 bits: 10 alternating bits to detect start,
      followed by 5 ones and 5 zeros to detect whether the following bits is a
      \\
    //--'0' or a '1'. A phase shift indicates a transition between 0 and 1. \\
101 //-- The remaining 30 bits is databits\\
    int test\_seq0[50] = \{\\
103   0,1,0,1,0,1,0,1,0,1,    // 10 Alternating bits to detect data stream\\
      1,1,1,1,1,0,0,0,0,0,    // 5 ones and 5 zeros to declare what is what\\
105   0,1,0,0,1,0,1,0,1,1,    // 30 databits\\
      0,1,0,1,0,0,0,1,1,0,\\
107   0,1,0,1,1,0,0,1,0,0\\
    \};\\
109 int test\_seq1[50] = \{\\
      0,1,0,1,0,1,0,1,0,1,    // 10 Alternating bits to detect data stream\\
111   1,1,1,1,1,0,0,0,0,0,    // 5 ones and 5 zeros to declare what is what\\
      1,1,0,1,0,1,0,0,0,1,    // 30 databits\\
113   0,0,1,0,1,1,1,0,0,1,\\
      0,0,1,1,0,1,1,0,0,1\\
115 \};\\
    int test\_seq2[50] = \{\\
117   0,1,0,1,0,1,0,1,0,1,    // 10 Alternating bits to detect data stream\\
      1,1,1,1,1,0,0,0,0,0,    // 5 ones and 5 zeros to declare what is what\\
119   0,0,1,0,0,1,1,0,1,0,\\
      1,1,0,1,0,1,1,1,0,1,\\
121   0,1,0,0,1,0,1,1,0,1\\
    \};\\
123 int test\_seq3[50] = \{\\
      0,1,0,1,0,1,0,1,0,1,    // 10 Alternating bits to detect data stream\\
125   1,1,1,1,1,0,0,0,0,0,    // 5 ones and 5 zeros to declare what is what\\
      1,1,0,0,1,0,1,1,0,1,\\
127   0,1,0,1,0,0,1,1,0,1,\\
      0,1,0,1,0,1,0,1,1,0\\
129 \};\\

131 while(1)\{  //Send test-sequence 0-3 with 0.237, 0.825, 11,7 and 40 kbps
      data rate and 5 seconds carrier between each\\

133   //Set data rate to approximately 237 bps, burst time is rougly 205ms\\
      SPI.setClockDivider(SPI\_CLOCK\_DIV128);  // 1/128 of the clock frequency
       \\
135   for (int i = 0; i < 50; i++)\{\\
        writeBPSK(test\_seq0[i]);\\
137     delay(4);       \\
      \}\\
139
      delay(1000);\\
141
      //Set data rate to approximately 825 bps\\
143   SPI.setClockDivider(SPI\_CLOCK\_DIV128);  // 1/128 of the clock frequency
       \\
      for (int n = 0; n < 3; n++)\{\\
145     for (int i = 0; i < 50; i++)\{\\
          writeBPSK(test\_seq1[i]);\\
147       delay(1);       \\
```

```
     \}\\
149  \}

151  delay(1000);  //send carrier for 5 seconds\\

153  //Set data rate to approximately 11,7 kbps\\
     SPI.setClockDivider(SPI\_CLOCK\_DIV32);  // 1/32 of the clock frequency\\
155  for (int n = 0; n < 48; n++)\{\\
       for (int i = 0; i < 50; i++)\{\\
157      writeBPSK(test\_seq2[i]);\\
         delay(0);  // Insert zero-delay to tune data rate\\
159      delay(0);      \\
         delay(0);      \\
161      delay(0);      \\
         delay(0);      \\
163      delay(0);  \\
       \}    \\
165  \}\\

167  delay(1000);  //send carrier for 5 seconds\\

169  //Set data rate to approximately 39,8 kbps\\
     SPI.setClockDivider(SPI\_CLOCK\_DIV4);  // 1/4 of the clock frequency\\
171  for (int n = 0; n < 190; n++)\{\\
       for (int i = 0; i < 50; i++)\{\\
173      writeBPSK(test\_seq3[i]);\\
       \}    \\
175  \}\\

177  delay(1000);  //send carrier for 5 seconds\\

179  // Transmit FSK with datarate of 11,7 kbps\\
     SPI.setClockDivider(SPI\_CLOCK\_DIV32);  // 1/32 of the clock frequency\\
181  for (int n = 0; n < 190; n++)\{\\
       for (int i = 0; i < 50; i++)\{\\
183      writeFSK(test\_seq3[i]);\\
       \}    \\
185  \}\\
     writeFSK(0);\\
187
     delay(1000);\\
189\}\\
\}
191
void initDDS()\{\\
193  //Reset DDS, active HIGH\\
     digitalWrite(RESET, HIGH);  \\
195  digitalWrite(RESET, LOW);\\

197  // Setup CFR1 (0x00) 0x00 00 00 00\\
     int CFR1\_inst[4] = \{\\
199    B00000000,    //b3    // Ram and assorted controls\\
       B00000000,    //b2    // Sync enables and Not used\\
201    B00000010,    //b1    // Auto-Clear Phase Accumulator <13>\\
       B00000000,    //b0    // Assorted power-downs\\
203  \};\\
     writeDDS(CFR1\_adr, CFR1\_inst, 4);\\
205
       //Setup CFR2 0x00 00 24\\
207  int CFR2\_inst[3] = \{\\
       0B00000000,    //b2    // Not used\\
```

```
    0B00000000,     //b1    // Disables high speed synch, HW manual synch and
     XTAL OUT\\
    0B00100100,     //b0    // REFCLK <7:3> multiplier = 4, VCO <2> range FULL
     \\
  \};\\
  writeDDS(CFR2\_adr, CFR2\_inst, 3);\\

  //Setup Frequency Tuning Word to get output frequency of 15 MHz\\
  int FTW0\_inst[4] = \{\\
    B00001001,     //b3    (0x00)\\
    B10011001,     //b2    (0x99)\\
    B10011001,     //b1    (0x99)\\
    B10011001,     //b0    (0x99)\\
  \};\\
 writeDDS(FTW0\_adr, FTW0\_5MHz, 4);\\
\}\\

void writeDDS(int adrReg, int instReg[], int numBytes)\{\\
  SPI.transfer(adrReg);  //Send adress\\

  for(int i = 0; i < numBytes; i++)\{ \\
    SPI.transfer(instReg[i]);  //Send instruction into adress register\\
  \}\\
  digitalWrite(IOUPDATE, HIGH);    //Load register into DDS\\
  digitalWrite(IOUPDATE, LOW);  \\
\}\\

void writeBPSK(int Bit)\{\\
  //--- Modulates 180 degree phase shift of the signal each time there comes
     an transistion between \\
  //--- '0' and '1'. \\
  if (Bit == 0)\{\\
    writeDDS(POW0\_adr, POW0\_0deg, 2);\\
  \} \\
  else\{\\
    writeDDS(POW0\_adr, POW0\_180deg, 2);\\
 \}\\
\}\\
void writeFSK(int Bit)\{\\
  //--- Modulates 180 degree phase shift of the signal each time there comes
     an transistion between \\
  //--- '0' and '1'. \\
  if (Bit == 0)\{\\
    writeDDS(FTW0\_adr, FTW0\_5MHz, 4);\\
  \} \\
  else\{\\
    writeDDS(FTW0\_adr, FTW0\_5\_1MHz, 4);\\
  \}\\
\}
```

B

Back-up BPSK-modulator Program

```
/*
  Back-up plan. This program sends out a test sequence on pin 6 from an
     Arduino Uno. \\
*/\\

//-----Declarations-----//\\
//--Pins\\
int OutputPin = 6;            // Serial Data input/output pin\\

void setup()\{\\
  //Declare pin as output and set low\\
  pinMode(OutputPin, OUTPUT); \\
  digitalWrite(OutputPin, LOW);\\
\}\\

void loop()\{\\
  int delayfactor200bps = 5;\\
  int delayfactor1000bps = 1;\\
  int delayfactor10000bps = 0;\\

  int test\_seq1[50] = \{    // 200 bps sequence\\
    0,1,0,1,0,1,0,1,0,1,    // 10 Alternating bits to detect data stream\\
    1,1,1,1,1,0,0,0,0,0,    // 5 ones and 5 zeros to declare what is what\\
    1,1,0,1,0,1,0,0,0,1,    // 30 databits randomly selected, evenly
     distributed between "0" and "1"\\
    0,0,1,0,1,1,1,0,0,1,\\
    0,0,1,1,0,1,1,0,0,1\\
  \};\\
  int test\_seq2[50] = \{    // 1 kbps sequence\\
    0,1,0,1,0,1,0,1,0,1,    // 10 Alternating bits to detect data stream\\
    1,1,1,1,1,0,0,0,0,0,    // 5 ones and 5 zeros to declare what is what\\
    0,0,1,0,0,1,1,0,1,0,    // 30 databits randomly selected, evenly
     distributed between "0" and "1"\\
    1,1,0,1,0,1,1,1,0,1,\\
    0,1,0,0,1,0,1,1,0,0\\
  \};\\
  int test\_seq3[50] = \{    // 10 kbps sequence\\
    0,1,0,1,0,1,0,1,0,1,    // 10 Alternating bits to detect data stream\\
    1,1,1,1,1,0,0,0,0,0,    // 5 ones and 5 zeros to declare what is what\\
    1,1,0,0,1,0,1,1,0,1,    // 30 databits randomly selected, evenly
     distributed between "0" and "1"\\
    0,0,0,1,0,0,1,1,0,1,\\
    0,1,0,1,0,1,0,1,1,0\\
  \};\\

  while(1)\{\\
```

```
43      BPSKmod(test\_seq1, delayfactor200bps);  // Send out 200 bps sequence\\
        delay(1000);  // Send carrier for 1 second\\
45      for (int i = 0; i < 5; i++)\{\\
          BPSKmod(test\_seq2, delayfactor1000bps);  // Send out 1000 bps sequence
         \\
47      \}\\
        delay(1000);  // Send carrier for 1 second\\
49
        for (int n = 0; n < 500; n++)\{\\
51      BPSKmod(test\_seq3, delayfactor10000bps);  // Send out 114 kbps sequence\\
        \}\\
53      delay(1000);  // Send carrier for 1 second\\
      \}\\
55  \}\\

57  void BPSKmod(int sequence[], int del)\{  //Takes inn a testsequence and a
         delayfactor to modulate with an appropriate rate\\

59    for (int i = 0; i < 50; i++)\{    \\
        if (sequence[i] == 0)\{    // Checks if the bit is either an "0" or a "1"
         and sets the pin HIGH or LOW\\
61        digitalWrite(OutputPin, LOW);\\
        \}\\
63      else\{\\
          digitalWrite(OutputPin,HIGH);\\
65      \}\\
        delay(del);    // Delay with appropriate delay factor in order to get
         desired datarate\\
67    \}\\
    \}
```

C

BPSK Decoder

```
%MATLAB BPSK Demodulation Program Customized to Demodulate a Baseband
%Sampled Signal from a .wav-file.
%Based on Sampling from a Signal with a Minor Clock Drift/Offset

function Output = BPSK_Demod(signal)
Fs = 5e5;       %Sampling frequency [S/s]
burstTime=0.220;  %Burst time approximately 220 ms
burstTimeInSamples=burstTime*Fs;
prompt = 'Input number of seconds after start for processing: ';
seconds=input(prompt);  %Store input from user
secondsInSamples=seconds*Fs;    %Convert start time to start sample

figure();   %Display figure for user
plot(signal(secondsInSamples:secondsInSamples+3e6,1));   %Show q-samples of
    input signal

%Specify data rate
prompt = 'Input wanted data rate (1=237, 2=825, 3=11641, 4=46598): ';
dataRate=input(prompt);   %Store input from user
switch dataRate
    case 1
        numberOfPackages=1;
        dataRate=237;
    case 2
        numberOfPackages=3;
        dataRate=825;
    case 3
        numberOfPackages=48;
        dataRate=11641;
    case 4
        numberOfPackages=190;
        %dataRate=39800;
        dataRate=46598;
    otherwise
        disp('You typed in an unvalid choice');
        return;
end

onebit = Fs/dataRate;  %Number of samples corresponding to one bit
disp('Number of samples per bit = ');
disp(onebit);
prompt = 'Input sample number indicating start of data burst: ';
burstStart=input(prompt);   %Store input from user
signalSamples=1e3*signal(burstStart:(burstStart+burstTimeInSamples),:); %Cut
    out burst samples
```

```
complex_samples=complex(signalSamples(:,1),signalSamples(:,2)); %Convert to
    complex numbers
Estimate offset frequency to generate reference signals
prompt = 'Input sample number of offset carrier peak 1: ';
peak1=input(prompt);  %Store input from user
prompt = 'Input sample number of offset carrier peak 2: ';
peak2=input(prompt);  %Store input from user
Fc=Fs/(peak2-peak1);    %Calculate clock offset frequency
disp('Estimated clock offset: ');
disp(Fc);
disp(' Hz');

scaleFactor=abs(complex_samples(100));

%Estimate offset angle from package start w.r.t. offset carrier
prompt = 'Input estimated offset in degrees from preceeding peak: ';
offsetDeg=input(prompt)+186;  %Store input from user
offsetRad=(offsetDeg*pi)/180;   %Convert offset from degrees to radians
b=round(onebit);    %Number of samples corresponding to one bit
incrementBit=0;
c=1;
n=50*numberOfPackages;   %Number of bits to decode
k=[];   %Initialize array of output bits
figure()

for m=1:n;  %Iteration from 1 to number of bits
    y=complex_samples((c+3):(b-3)); %Take out the needed signal for one bit

    %Generate reference signals - Quadrature
    q1=cos(2*pi*(((c+3):(b-3))-1)*Fc/Fs);
    q2=sin(2*pi*(((c+3):(b-3))-1)*Fc/Fs);
    q=scaleFactor*complex(q1,-q2).*exp(1i*offsetRad);

    %Generate reference signals - Inphase
    i1=-cos(2*pi*(((c+3):(b-3))-1)*Fc/Fs);
    i2=-sin(2*pi*(((c+3):(b-3))-1)*Fc/Fs);
    i=scaleFactor*complex(i1,-i2).*exp(1i*offsetRad);

    %Multiply input signal with reference signal
    q_test=y.'+q;
    i_test=y.'+i;
    t=sum(abs(q_test))-sum(abs(i_test));
    if t<0
        p=0; %Create output (0) for the length of one bit
    else
        p=1; %Create output (1) for the length of one bit
    end
    if 0 < m & 4 > m
        hold on;
        %plot(q_test,'b');
        %plot(i_test,'r');
        plot(y,'g');
        plot(q,'b');
        plot(i,'r');
        xlabel('Q');
        ylabel('I');

        %For decoder plotting
        %str=('BPSK Demodulation with Reference Signal Reconstruction');
        %title(str);
```

```
        %hleg1 = legend('0-curve Correlated with Signal','1-curve Correlated
    with Signal','Sampled Signal');
        %set(hleg1,'Location','NorthEast')
        %set(hleg1,'Interpreter','none')
    end
    c;
    signalSamples(c,1)/(1e3);
    k=[k p];    %Accumulate the value of output into k
    incrementBit=incrementBit+onebit;
    c=round(incrementBit); %Update the value of c for the next input
    b=round(incrementBit+onebit); %Update the value of b for the next input
end

hold off;
A = sequenceTest(k, dataRate);
if length(A)>0
disp('First wrong sample: ');
disp(A(1));
end
Output=k;  %Return output vector with demodulated bits
end
```

```
%%sequenceTest.m
%/Checks a stream of decoded bits to the original sent bits
%Returns the number of wrong bits and also which bits that was wrong

function result = sequenceTest(decodedBitVector, dataRate)

switch dataRate
     case 237
        refOutput=[0,1,0,1,0,1,0,1,0,1, 1,1,1,1,1,0,0,0,0,0,
    0,1,0,0,1,0,1,0,1,1, 0,1,0,1,0,0,0,1,1,0, 0,1,0,1,1,0,0,1,0,0];
        n=1;
    case 825
        refOutput=[0,1,0,1,0,1,0,1,0,1, 1,1,1,1,1,0,0,0,0,0,
    1,1,0,1,0,1,0,0,0,1, 0,0,1,0,1,1,1,0,0,1, 0,0,1,1,0,1,1,0,0,1];
        n=3;
        %n=1;
    case 11641
        refOutput=[0,1,0,1,0,1,0,1,0,1, 1,1,1,1,1,0,0,0,0,0,
    0,0,1,0,0,1,1,0,1,0, 1,1,0,1,0,1,1,1,0,1, 0,1,0,0,1,0,1,1,0,1];
        %n=48;
        n=1;
    case 46598 %39800
        refOutput=[0,1,0,1,0,1,0,1,0,1, 1,1,1,1,1,0,0,0,0,0,
    1,1,0,0,1,0,1,1,0,1, 0,1,0,1,0,0,1,1,0,1, 0,1,0,1,0,1,0,1,1,0];
        %n=190;
        n=1;
    otherwise
        disp('Unknown data rate');
        return;
end

%Create extended reference vector equal to the lengths of the input vector
refOutputTest=[];
for j=1:n
    refOutputTest=[refOutputTest refOutput];
end
length(refOutputTest)

%Check bits in input vector versus reference
```

```
rightBits=0;
wrongBits=0;
result=[];
for i=1:(50*n)
   if decodedBitVector(i)==refOutputTest(i)
       rightBits=rightBits+1;
   else
       wrongBits=wrongBits+1;
       result=[result i];
   end
end
rightBits
wrongBits
end
```

D

SDR Recordings

D.1 Recorded SDR Output

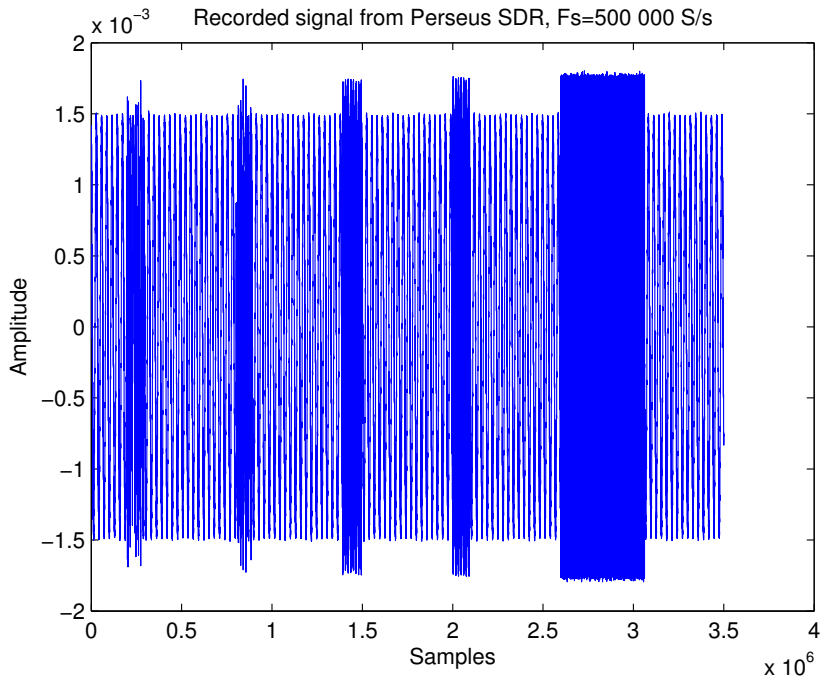

FIGURE D.1: Recorded Waveform from Primary Hardware. 4 BPSK Modulated Bursts with Rates of 237 bps, 825 bps, 11.641 kbps and 46.598 kbps, Followed by 1 FSK Burst with 10 kbps Rate

D.2 SDR Output with Frequency Offset

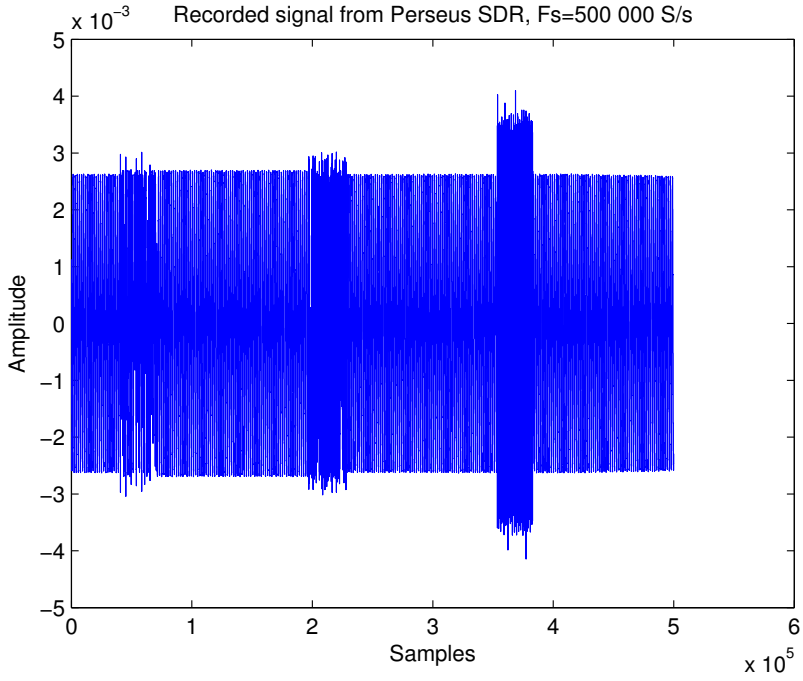

FIGURE D.2: Test Sequence from Back-up Hardware. 3 BPSK Modulated Bursts with Rates of 200 bps, 1 kbps and 114 kbps Respectively

E

Test Locations

E.1 Location I

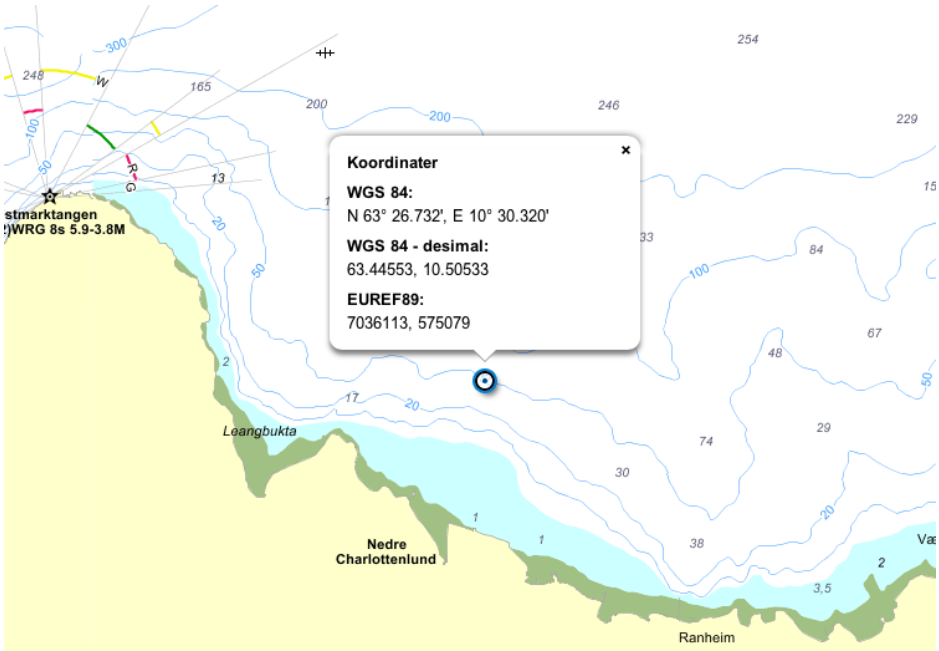

FIGURE E.1: Sea Test Location I.

E.2 Location II

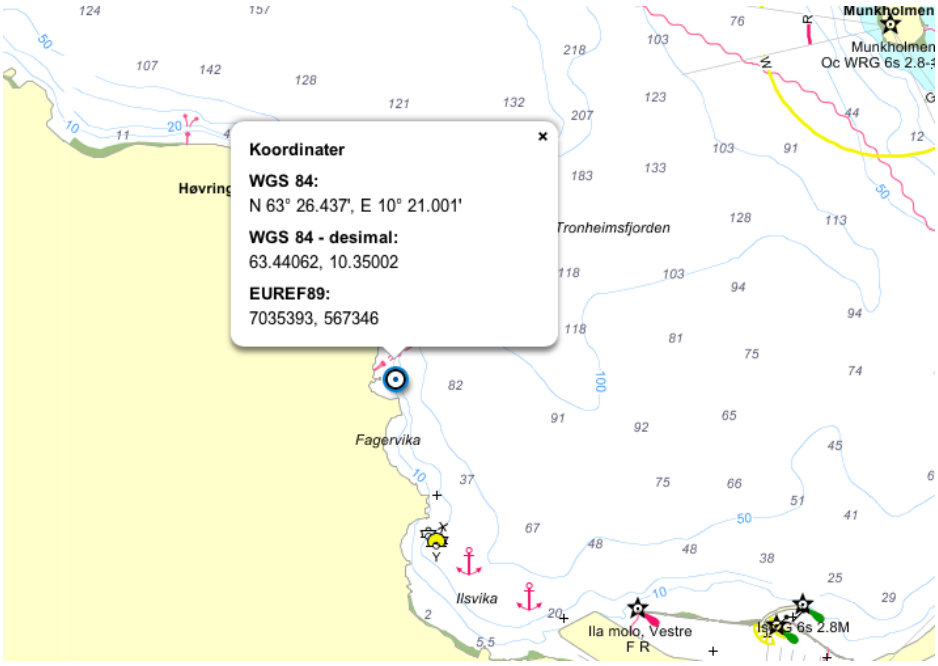

FIGURE E.2: Sea Test Location II.

Bibliography

Al-Shamma'a, A., Shaw, A. & Saman, S. [2004], 'Propagation of electromagnetic waves at MHz frequencies through seawater', *Antennas and Propagation, IEEE Transactions on* **52**(11), 2843 – 2849.

Analog Devices [2009], 'AD9954 Data Sheet Rev B, 05/2009', `http://www.analog.com/static/imported-files/data_sheets/AD9954.pdf`. Accessed May 24. 2013".

Analog Devices [2010], 'ADM232A Data Sheet Rev B', `http://www.analog.com/static/imported-files/data_sheets/ADM222_232A_242.pdf`. Accessed May 4. 2013".

Arduino [2013*a*], 'Arduino - ArduinoBoardUno', `http://arduino.cc/en/Main/ArduinoBoardUno`. Accessed May 3. 2013".

Arduino [2013*b*], 'Arduino - SPI', `http://arduino.cc/en/Reference/SPI`. Accessed May 9. 2013".

Balanis, C. A. [2005], *Antenna Theory Analysis and Design*, third edn, John Wileys & Sons, Inc, New Jersey.

Chamberlain, M. [2005], A software defined HF radio, *in* 'Military Communications Conference, 2005. MILCOM 2005. IEEE', pp. 2448–2453 Vol. 4.

Couch II, L. W. [1995], *Modern Communication Systems - Principles and Applications*, first edn, Prentics Hall, New Jersey.

Ellison, W., Balana, A., Delbos, G., Lamkaouchi, K., Eymard, L., Guillou, C. & Prigent, C. [1998], 'New permittivity measurements of seawater', *Radio Science* **22**(3), 634–648.

Fairchild Semiconductor [2013], 'LM78XX/LM78XXA 3-Terminal 1A Positive Voltage Regulator', `http://www.fairchildsemi.com/ds/LM/LM7805.pdf`. Accessed May 3. 2013".

Fjuk, P. O. E. [2012], 'Underwater Radio Communication using Wideband Biconical Antennas'. TFE4540 Specialization Project.

IQD Frequency Products [2012], 'Oscillator Specification, Model: IQXO-350', `http://www.iqdfrequencyproducts.com/products/details/iqxo-350-20-03.pdf`. Accessed May 4. 2013".

Ismail, M. Z. [2013], '2 Level PSK Demodulator with Sampling Frequency, Carrier Frequency and Bitrate', `http://www.mathworks.com/matlabcentral/`

fileexchange/25243-bpsk-demodulator/content/bpsk.m. Accessed May 28. 2013".

Kongsberg Maritime [2012], 'cPAP - Subsea transceiver for ROV'. Accessed April 30. 2013".
URL: *http://www.km.kongsberg.com/ks/web/nokbg0397.nsf/AllWeb/BFF2F9698C59286DC1257A9200315A83/$file/355125_cpap_product_specification.pdf*

Lucas, J. & Yip, C. K. [2007], 'A determination of the propagation of electromagnetic waves through seawater', *Underwater Technology: The International Journal of the Society for Underwater* **27**(1), 1–9.

Madhow, U. [2008], *Fundamentals of Digital Communications*, first edn, Cambridge University Press, Cambridge.

Microtelecom s.r.l. [2013*a*], 'Perseus Receiver User Manual', http://microtelecom.it/perseus/perseususermanual-en14.pdf. Accessed May 3. 2013".

Microtelecom s.r.l. [2013*b*], 'Perseus SDR Home Page', http://microtelecom.it/perseus/. Accessed May 2. 2013".

Mini-Circuits [2013], 'Mini-Circuits', http://217.34.103.131/pdfs/ZMAS-3.pdf. Accessed May 3. 2013".

Mini Kits [2013], 'Basic AD9945 DDS VFO', http://www.minikits.com.au/electronic-kits/dds-synthesizer/basic-dds/Basic-AD9954-DDS. Accessed May 3. 2013".

More, R. K. [1967], 'Radio communication in the sea', *IEEE Spectrum* **4**, 42–51.

Northrup Corporation [1966], 'Underwater radio communication', *Wireless World* **73**, 80.

Pettersen, M. & Husoey, T. S. [2012], 'cNODE - an Integrated Seabed Platform for Underwater Research', http://www.ucomms.net/Proceedings/Pettersen_Husoey.pdf. Accessed May 30. 2013".

Pozar, D. M. [2001], *Microwave and RF Design of Wireless Systems*, first edn, John Wileys & Sons, Inc, New Jersey.

Proakis, J. G. & Salehi, M. [2008], *Digital Communications*, fith edn, McGraw-Hill, New York.

Rappaport, T. S. [2002], *Wireless Communications: Principles and Practice*, second edn, Prentics Hall, New Jersey.

RF Bay Inc. [2013], 'MPA-10-40', `http://rfbayinc.com/products_pdf/product_185.pdf`. Accessed May 3. 2013".

Rhodes, M. & Hyland, B. [2009], 'Underwater communications'.

Shaw, A., Al-Shamma'a, A., Wylie, S. & Toal, D. [2006], Experimental investigations of electromagnetic wave propagation in seawater, *in* 'Microwave Conference, 2006. 36th European', pp. 572 –575.

Siegel, M. & King, R. W. P. [1973], 'Electromagnetic Propagation Between Antennas Submerged in the Ocean', *IEEE Transactions on Antennas and Propagation* **21**, 507–513.

Ulaby, F. T., Michielssen, E. & Ravaioli, U. [2007], *Fundamentals of Applied Electromagnetics*, sixth edn, Prentice Hall, New Jersey.

WFS Technologies [2012], 'Seatooth', `http://www.wfs-tech.com/images/uploads/seatooth_overview_US_1.pdf`. Accessed June 5. 2013".

Yip, C. K., Goudevenos, A. & Lucas, J. [2008], 'Antenna design for the propagation of EM waves in seawater', *Underwater Technology: The International Journal of the Society for Underwater* **28**(1), 11–20.